CCR2: Characterization of the Antagonist Binding Site from a Combined Receptor Modeling/Mutagenesis Approach

Theo A. Berkhout,[†] Frank E. Blaney,*[,‡] Angela M. Bridges,[§] David G. Cooper,[‡] Ian T. Forbes,[‡] Andrew D. Gribble,[‡] Pieter H. E. Groot,[†] Adam Hardy,[†] Robert J. Ife,[‡] Rejbinder Kaur,[†] Kitty E. Moores,[†] Helen Shillito,[†] Jennifer Willetts,[§] and Jason Witherington[‡]

Departments of Discovery Chemistry, Vascular Biology, and Gene Expression Sciences, GlaxoSmithKline, New Frontiers Science Park, Third Avenue, Harlow, Essex, UK CM19 5AD

Received April 4, 2003

We describe here a classical molecular modeling exercise that was carried out to provide a basis for the design of novel antagonist ligands of the CCR2 receptor. Using a theoretical model of the CCR2 receptor, docking studies were carried out to define plausible binding modes for the various known antagonist ligands, including our own series of indole piperidine compounds. On the basis of these results, a number of site-directed mutations (SDM) were designed that were intended to verify the proposed docking models. From these it was clear that further refinements would be necessary in the model. This was aided by the publication of a crystal structure of bovine rhodopsin, and a new receptor model was built by homology to this structure. This latest model enabled us to define ligand-docking hypotheses that were in complete agreement with the results of the SDM experiments.

Introduction

Chemokines are small, inducible, secreted chemotactic cytokines involved in the trafficking of white blood cells, critical in immunosurveillance and inflammation.[1] On the basis of the configuration of conserved cysteine residues, four classes can be distinguished: CXC, CC, CX3C, and C chemokines. Chemokines exert their effects via activation of specific receptors that belong to the superfamily of G protein-coupled transmembrane spanning receptors. Many chemokine receptors are promiscuous in ligand interaction, but they are selective insofar that all accepted ligands are of the same chemokine class. On the basis of their ligand preference, receptors have been classified as CC, CXC, CX3C, and C chemokine receptors. Recently, the IUPHAR nomenclature system for chemokines and their receptors has been published.[2]

The CC-chemokine receptor 2 (CCR2) is expressed on monocytes and recognizes the ligands MCP-1, MCP-2, MCP-3, and MCP-4.[3] In the past decade, much evidence has emerged suggesting a pathological role of MCP-1 and CCR2 in diseases involving chronic inflammation, in particular atherosclerosis.[4] Thus, MCP-1 has been shown to be highly expressed in human and mouse atherosclerotic lesions by in situ hybridization or immunostaining.[5] Furthermore, mice in which the genes for MCP-1 or CCR2 have been silenced and bred on an apoE -/- or LDL receptor -/- background[6] show a substantial reduction in atherosclerotic lesions, while overexpression of mouse MCP-1 (JE) in apoE -/- mice was found to exacerbate the disease.[7] It has also been reported that a truncated antagonist analogue of MCP-1 (MCP-1 9−76) prevented the onset of arthritis in the MRL-lpr mouse model.[8] These data suggest that lowering MCP-1 levels, or blocking CCR2, in man may have useful therapeutic effects in treating chronic inflammatory conditions such as atherosclerosis and/or arthritis. The discovery and development of small molecular weight CCR2 antagonists has therefore been regarded as an important pharmaceutical opportunity.

Over the past few years, there have been major advances in the discovery of small molecule antagonists of chemokine receptors.[9] With regard to CCR2, four chemically distinct series of antagonists have been reported (Scheme 1). The cinnamide **1** (SB-282241)[10] is a potent functional antagonist of CCR2, but suffers from lack of selectivity over 5-HT receptors. The spiropiperidine **2** (RS-504393)[11] has equal affinity at the α_{1B} adrenoceptor and also has lower functional potency than would be predicted from its binding affinity. Several publications from Takeda have highlighted the CCR5 receptor antagonist **4** (TAK-779),[12] which also possesses significant activity at the CCR2 receptor. Acceptable bioavailability of this quaternary salt may be an issue, so clearly the profile of the corresponding free base **3** is also of interest (vide infra). A series of amide derivatives have been reported from Teijin as possessing CCR2 antagonist activity, with **5** being identified as a lead compound.[13] Both compounds **2** and **5** are reported to have poor affinities at rodent CCR2 receptors, making biological evaluation of these compounds difficult.

Thus, despite intense interest in the development of CCR2 antagonists as potential drug candidates, the

* To whom correspondence should be addressed. Phone: (+)44 1279 622143. Fax:(+)44 1279 622790. Email:frank_e_blaney@gsk.com.
[†] Department of Vascular Biology.
[‡] Department of Discovery Chemistry.
[§] Department of Gene Expression Sciences.

10.1021/jm030862l CCC: $25.00
Published on Web 08/13/2003

Scheme 1. Structures of CCR2 Antagonists and Their Published Affinities

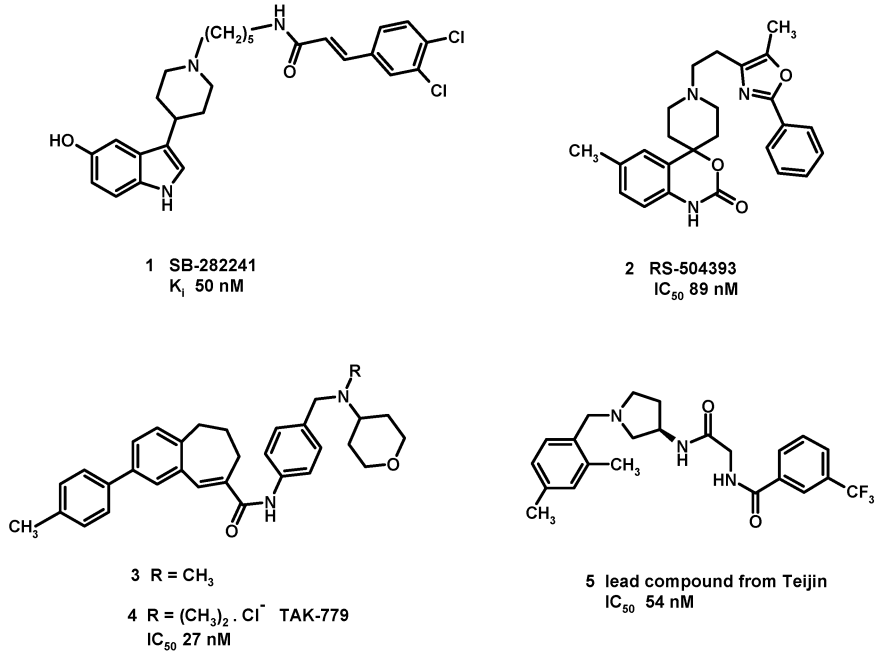

Scheme 2. Synthesis of 1 (SB-282241)[a]

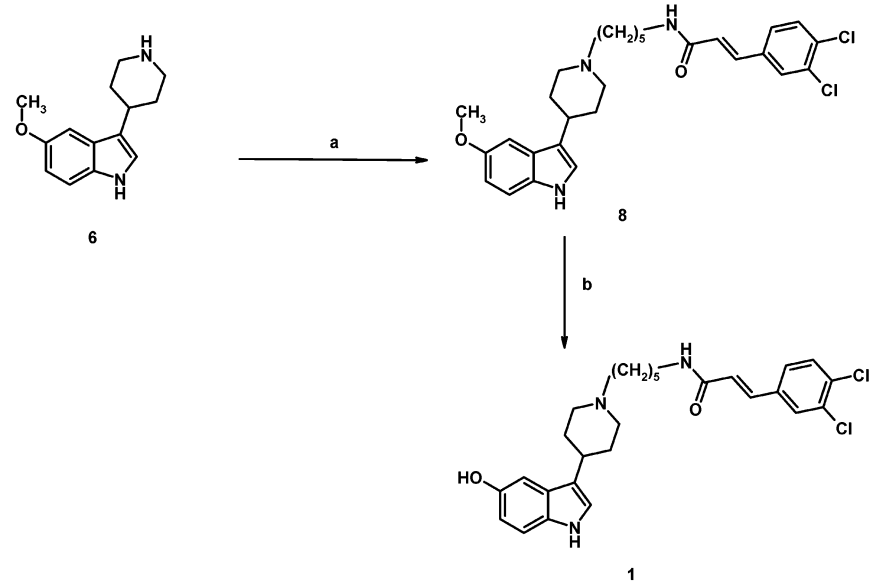

[a] Reagents: (a) $Br(CH_2)_5NHCOCH{=}CHPh(3,4\text{-}Cl_2)$ (**7**), $NaHCO_3$, DMF, 80 °C, 7 h (89%); (b) pyridine hydrochloride, sealed tube, 130 °C, 48 h (40%).

identification of potent and selective compounds possessing suitable pharmacokinetic properties still remains an unmet challenge for the pharmaceutical industry. With the goals of gaining a fuller understanding of the nature of the interactions of diverse ligands with the CCR2 receptor and thus identifying a pharmacophore for antagonists at CCR2, we embarked upon a combined modeling/SDM approach to aid the design of novel structures possessing a profile superior to those of the existing leads.

Chemistry

Compound **1** (SB-282241) was synthesized as shown in Scheme 2. Alkylation of 4-(5-methoxyindol-3-yl)-piperidine **6**[14] with the bromide **7** afforded the intermediate **8**, which was demethylated using pyridine hydrochloride to afford the final product **1**.

Compound **2** (RS-504393) was synthesized as shown in Scheme 3. Ortho lithiation of BOC-protected 2-bromo-4-methylaniline **9** followed by reaction with *N*-BOC-4-piperidone yielded the spiro intermediate **10**, which was deprotected using ethanolic hydrogen chloride to afford **11**. Alkylation of **11** with the bromide **12** provided the target compound **2**.

Compounds **3** and **4** were prepared as described by Takeda.[12]

Compound **5** (Teijin lead) was synthesized as indicated in Scheme 4. Reductive alkylation of 2,4-dimethylbenzaldehyde **12** with *R*-3-*tert*-butyloxycarbonylami-

Scheme 3. Synthesis of 2 (RS--504393).[a]

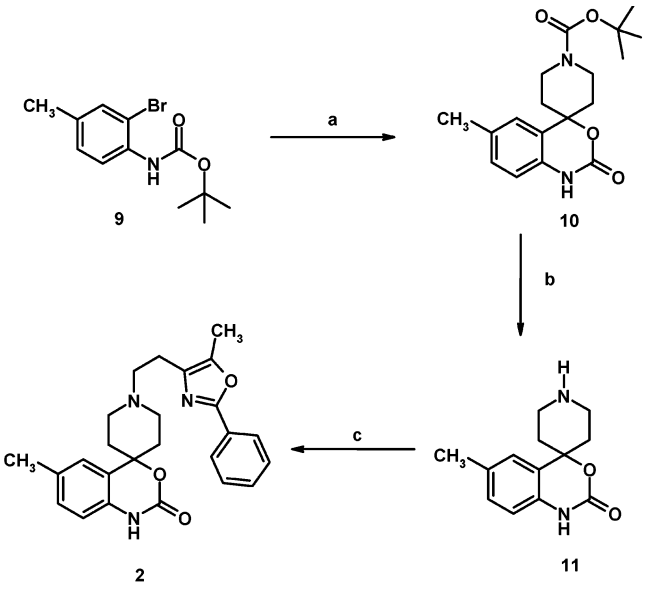

[a] Reagents: (a) MeLi, ^{t}BuLi, THF, −78 °C, *N*-^{t}BOC-piperidone, room temperature, 18 h, (52%); (b) EtOH/HCl, room temperature, 1 h (95%); (c) 4-bromoethyl-5-methyl-2-phenyl-1,3-oxazole **12**, $NaHCO_3$, DMF, 60 °C, 4 h (78%).

nopyrrolidine **13** provided the intermediate **14**. Deprotection of **14** followed by standard carbodiimide coupling with BOC-glycine afforded the homologated amide **15**, which was similarly deprotected to **16** and coupled with 3-trifluoromethylbenzoic acid, to furnish the target structure **5**.

Biology

Initially, the four chemical series indicated above were fully profiled on binding and functional studies in our own laboratories, as comparative data for all compounds were required prior to our mutation studies discussed below. Compounds **1**−**5** were evaluated for their ability to inhibit MCP-1 binding to membranes of CHO cells stably expressing CCR2 (12000 receptors/cell). For functional studies, inhibition of MCP-1-stimulated chemotaxis of freshly isolated peripheral human monocytes was investigated. The binding displacement data and the chemotaxis data are expressed as pK_i and pK_b values, respectively (Table 1),[15] and are in close agreement with literature data, where available. As can be seen from Table 1, compounds **1**−**5** display a range of different binding affinities at CCR2, with **4** (TAK-779) representing the most potent analogue and **5** (Teijin lead) representing the least potent. Unexpectedly, the free base **3** is ca. 10-fold less potent than the quaternized form **4** (TAK-779), perhaps indicating a difference in the way that these two compounds interact with the receptor. In the functional assay, the antagonist profile of **1**−**5** was confirmed**.** However, compounds **1**−**4** are up to 10-fold more potent than in the binding assay, but the same rank order of affinities is maintained. Interestingly, the Teijin lead **5** does not display this increased functional potency, possessing a similar pK_i and pK_b.

Table 1. Inhibition of Binding and Chemotaxis by CCR2 Antagonists[a]

	antagonist	binding pK_i ± SEM	chemotaxis pK_b ± SEM
1	SB-282241	7.30 ± 0.025 (n = 28)	7.71 ± 0.1 (n = 3)
2	RS-504393	6.68 ± 0.13 (n = 3)	7.57 ± 0.09 (n = 3)
3	TAK-779 base	7.54 ± 0.07 (n = 4)	8.63 ± 0.11 (n = 3)
4	TAK-779	8.38 ± 0.14 (n = 8)	9.53 ± 0.15 (n = 3)
5	Teijin lead	6.54 ± 0.13 (n = 4)	6.40 ± 0.25 (n = 3)

[a] Binding displacement of ^{125}I-MCP-1 (0.14 nM) was measured on CHO cell membranes expressing human CCR2. Inhibition of chemotaxis in human monocytes was measured in the presence of 1 nM MCP-1. TAK-799 base represents the free base of TAK-799.

CCR2 Receptor Modeling and Ligand Docking. The initial model of the CCR2 receptor was based on a template of frog rhodopsin that, in turn, was derived from published cryoelectron diffraction data at 6 Å resolution.[16] In these papers, electron density was depicted as a series of slices at 4 Å intervals going through the plane of the membrane. Using a recently published algorithm,[17] these density slices were converted into a set of three-dimensional images, which were used to define the helical axes of the transmembrane domain. The rhodopsin sequence was then folded ab initio around these axes, using experimental information on the relative positioning of key residues in the

Scheme 4. Synthesis of 5 (Teijin lead).[a]

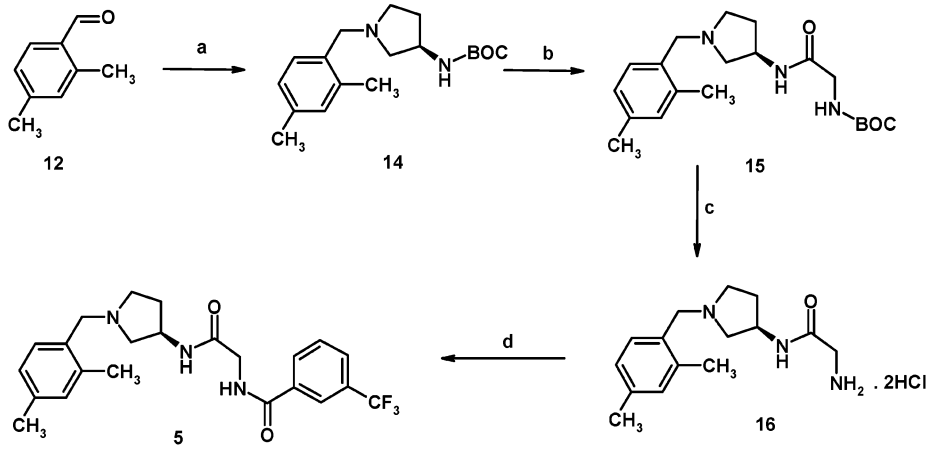

[a] Reagents: (a) *R*-3-^{t}butyloxycarbonylamino-pyrrolidine 13, sodium triacetoxyborohydride, 1,2-dichloroethane, room temperature (89%); (b) (i) EtOH/HCl, room temperature, 1 h (∼100%), (ii) *N*-^{t}BOC-glycine, diisopropylcarbodiimide, HOBT, DMF, room temperature, 18 h (56%); (c) EtOH/HCl, room temperature, 1 h (∼100%); (d) 3-trifluoromethylbenzoic acid, diisopropylcarbodiimide, HOBT, DMF, room temperature, 18 h (53%).

bundle. The positioning of conserved prolines in transmembrane (TM) helices 5 and 6 was facilitated by the presence of well-defined kinks in the two helical axes. This TM bundle was then used as a template to construct the CCR2 receptor model, using the automated GPCR_Builder program[18] developed some years ago in our laboratory. This whole process, as used in the construction of neurokinin receptor models, has been described in greater detail in a recent publication in this journal.[17] Once the TM domain of the CCR2 model was complete, the extracellular loops (ECLs) were then added using the following procedure. Essentially, a distance geometry approach (DGEOM95[19]) using constraints between consecutive helices, the known disulfide bond between TM3 and the second extracellular loop, and already constructed adjacent loops was used to generate 1000 random conformations for each loop (in order of increasing size, i.e., ECL1, ECL3, and ECL2). Each of these was minimized with CHARMm[20] using 300 steps of steepest descent (SD) followed by 3000 steps of adopted basis Newton Raphson (ABNR), keeping the helical ends of the loop region fixed. The resulting conformations were initially ranked by the number of violations in backbone dihedral (Ramachandran) space. In the case of the CCR2 loops, a sufficient number of conformations were found with no violations. These were ranked in order of increasing energy and the lowest 10 were subjected to molecular dynamics simulations using the locally enhanced sampling procedure[21] implemented in CHARMm (five copies, 1 ns sampling time, and 400 K). The loop family showing the greatest convergence of conformation and with no backbone violations was chosen as the final structure. The diverse ligands under study all contain a basic positively charged center and this was therefore assumed to interact with the glutamate residue (E291) on TM7 (see Discussion). The ligands used in this study were initially built using the Spartan program[22] and were further optimized at the semiempirical AM1 level using the Vamp program.[23] Atom centered point charges used in the molecular mechanics docking and optimization were ab initio natural atomic orbital charges, calculated with Spartan using a 3-21G* basis set. Electrostatic potential calculations (see Discussion) were also calculated with Spartan using this same basis set. The initial pharmacophore model was generated using manual rms fitting of key features such as the basic centers, hydrogen-bond acceptors, and hydrophobic regions. The result was very similar to the pharmacophore generated by Catalyst,[24] which is the program we routinely use for database searching. Automated docking programs are extensively used within our group for the placement of ligands, and a number of these were tried out in the case of the CCR2 model. For reasons that will be described in the Discussion, they have not been found to be successful with many 7TM receptors, and manual docking has therefore been used for the work described here. Each ligand was docked manually into the receptor in a variety of starting orientations, allowing only low-energy starting rotameric conformations for the ligand. Each placement of the ligand was accompanied by adjustment of the side chain dihedrals of the residues in the binding pocket, again only using the allowed rotamers found in the Karplus rotamer library.[25] The complexes were then fully minimized (500 steps of SD followed by 5000 steps of ABNR) with the CHARMm program.[20] Helical NOE distance constraints within the range of 1.8−2.5 Å for the i to $i + 4$ hydrogen bonds were used to maintain the TM bundle. These were generated using a CHARMm stream file that skipped the ith residue when it was a proline. Using this distance range allows the helix to adopt other conformational forms such as a 3/10 helix conformation or a proline kink. With the exception of these distance constraints, the receptor−ligand complex was allowed to fully relax. In all cases, several binding orientations were found to be possible. The residues in the model that were found to have significant interactions were used as the basis for deciding upon which SDM experiments to carry out (see Discussion for details).

After the initial modeling work, the X-ray crystal structure of bovine rhodopsin was published.[26] The crystal structure turned out to be remarkably similar to our model of rhodopsin. TM helices 3, 6, and most of 7 aligned almost perfectly with the crystal based models. Helices 1 and 2 were correctly oriented toward the inner face of the bundle but were approximately displaced by one helical turn in the transmembrane axis. Helices 4 and 5 were correct in their placement in the membrane axis but the inward faces were out by approximately 60°. In our previous work, this has proved to be fortuitous because ligand binding very often occurs primarily between TM3, TM6, and TM7. We have used these earlier rhodopsin-based models successfully in the design of ligands for serotonin[27] and neurokinin[17] receptors. In the case of CCR2, however, significant binding influences were found in TM1 and TM5. The main differences affecting the model structure were the relative placements of the TM1 tyrosine (Y49) and the TM5 arginine (R206). The crystal structure was used to rebuild a refined model of the CCR2 receptor, using the homology building tools within the Quanta program.[28] Once again the extracellular loop regions were added using the procedure described earlier. Using the information from the results of these SDM studies, the various ligands were redocked into this new model in orientations that would best explain the experimental data.

Plasmid Construction and Site-Directed Mutagenesis. Full-length cloning of the wild-type MCP1/CCR2 gene has been published.[3] The mutants chosen on the basis of the early receptor modeling were mainly in TM7, TM3, and TM1. Their relative positions in these helices are identified in Table 3 using the numbering scheme of Ballesteros and Weinstein,[29] together with their actual numbering in the sequence. The latter numbering will be used to simplify the discussion below, although the alternative positioning will also be given where appropriate. Mutants Y49F, Y120A, H121A, H121F, D284A, Q288A, E291Q, T292A, Y120A/T292A, and H121A/T292A were introduced using the QuickChange PCR-based mutagenesis kit (Stratagene) according to the manufacturer's protocol, using the wild-type expression vector, pCDNA3.1-MCP1, as the template

Table 2. PK_d Values for ^{125}I-MCP-1 Binding to Mutant CCR2 Receptors[a]

receptor variant	receptors/cell ± SEM	mean pK_d ± SEM	pK_d comparison with WT *t*-test[b]
WT	9027 ± 1815	10.18 ± 0.13	
Y49F	6949 ± 1082	10.01 ± 0.05	ns
Y120A	4758 ± 1167	9.99 ± 0.01	ns
H121A	9984 ± 2950	10.22 ± 0.13	ns
H121F	5093 ± 2206	10.47 ± 0.13	ns
D284A	7212 ± 1711	10.03 ± 0.12	ns
Q288A	12440 ± 1696	9.78 ± 0.24	$P \leq 0.05$
T290A	8552 ± 2161	10.10 ± 0.13	ns
E291Q	9390 ± 2668	9.02 ± 0.15	P 0.001
T292A	10369 ± 4827	10.09 ± 0.17	ns
Y120A/T292A	5202 ± 1402	9.56 ± 0.25	P 0.05
H121A/T292A	9152 ± 1043	10.26 ± 0.29	ns

[a] K_d values were determined from binding saturation experiments using single site, saturation curve fitting Grafit 4 software and converted to pK_d values. Data presented are results from at least three independent transfections. [b] Significance compared to wild type using a *t*-test for each comparison, assuming equal variances; ns = no significant difference.

for mutagenesis. The accuracy of all PCR-derived sequenceswas confirmed by dideoxy sequencing of the mutant plasmids. Constructs were transfected into HEK 293 cells using lipofectAMINE Plus (Life Technologies, Inc.) according to the manufacturer's protocol, and after 48 h, cell membranes were isolated for binding studies.

Evaluation of Receptor Mutants. The eleven CCR2 mutant receptors shown in Table 2 were characterized by establishing the receptor expression levels and the affinity for MCP-1 (pK_d) and by comparing these data with those obtained from the wild type CCR2 receptor expressed in the same transient cell line (HEK 293). It can be seen from Table 2 that the receptor expression levels were broadly similar, ranging from ~5000 to 12000 receptors per cell, compared to ca. 9000 receptors per cell for wild type. Generally, the affinity for MCP-1 did not vary significantly between wild type and mutant receptors, with the exception of E291Q, where there was a 10-fold reduction. This implies that MCP-1 has a significant but not crucial interaction with the glutamic acid residue at position 291, but not with any of the other amino acid residues under investigation. Thus, with these 10 mutant receptors we had suitable receptor densities and MCP-1 affinities for the purposes of our comparative studies below.

Having established that MCP-1 binds in a manner similar to wild type and all mutant receptors, the binding profile of compounds **1**−**5** across all mutant receptors was then investigated, using inhibition of ^{125}I-MCP-1 binding. The data obtained are shown in Tables 3 and 4, and a chart of key differences in affinities between wild type and mutant receptors for compounds **1**−**5** are displayed in Figures 1 (single mutants) and 2 (double mutants).

It is readily observed from Table 3 and Figure 1 that the most striking effects are observed with all five compounds on E291Q, in which the affinities of **1**, **2**, and **5** are reduced by over 100-fold, and the affinities of **3** and **4** are reduced by ca. 30-fold. A small but significant decrease in affinity was observed with compounds **1**, **2**, **3**, and **5** at the D284A mutant. As will be described later (see Discussion), this is probably not due to direct ligand receptor interactions with this residue but rather to a decrease in the electronegative environment of the ligand binding pocket. These data support the hypothesis that the glutamic acid residue at position 291, but not the aspartic acid residue at position 284, is involved in a key interaction with all ligands examined to date and extends the results reported from Roche,[13] in which E291Q and E291A mutations were shown to cause a pronounced decrease in affinity with their lead compounds. The adjacent threonine residue at position 292 is also an important residue in the receptor for binding of **1**−**5**, since affinities of **2**, **3**, and **5** are reduced by 10−30-fold and affinities of **1** and **4** are reduced by a lesser but significant amount, in the T292A mutant receptor. Compounds **2**−**4** exhibit a major reduction in affinity at the Y120A mutant receptor (10−100-fold), with a smaller reduction (<10-fold) observed with compounds **1** and **5**. No significant effects were seen at the Q288A mutant receptor. Major differences between the diverse series represented by **1**−**5** are apparent with His 121 and Tyr 49 mutations. Thus, compounds **1**, **2**, and **5** show typically 10-fold reduction in affinity at the H121A mutant receptor but possess relatively unchanged af-

Table 3. Profile of Antagonists Across Mutant CCR2 Receptors[a]

		pK_i				
receptor variant	residue position[b]	**1** (SB-282241)	**2** (RS-504393)	**3** (TAK-779 base)	**4** (TAK-779)	**5** (Teijin)
WT		7.00 ± 0.09	6.66 ± 0.016	7.16 ± 0.10	8.16 ± 0.12	6.47 ± 0.04
Y49F	Y1:39	7.78 ± 0.16	7.23 ± 0.15	6.82 ± 0.06	7.56 ± 0.08	6.50 ± 0.11
Y120A	Y3:32	6.25 ± 0.19	ia	5.59 ± 0.09	6.98 ± 0.13	5.74 ± 0.17
H121A	H3:33	5.60 ± 0.15	5.60 ± 0.09	6.52 ± 0.15	7.75 ± 0.10	5.59 ± 0.05
H121F	H3:33	6.78 ± 0.04	6.35 ± 0.26	7.62 ± 0.03	8.58 ± 0.13	6.18 ± 0.09
D284A	D7:32	6.64 ± 0.06	6.07 ± 0.03	6.23 ± 0.25	7.90 ± 0.20	6.14 ± 0.20
Q288A	Q7:36	6.77 ± 0.10	6.76 ± 0.20	6.64 ± 0.22	8.01 ± 0.13	6.50 ± 0.16
T290A	T7:38	6.89 ± 0.23*	6.28 ± 0.13*	6.98 ± 0.47	7.67 ± 0.53	NT
E291Q	E7:39	ia	ia	5.69 ± 0.24	6.83 ± 0.16	ia
T292A	T7:40	6.14 ± 0.10	5.20 ± 0.09	6.12 ± 0.12	7.54 ± 0.13	5.11 ± 0.04

[a] HEK 293 cells were transiently transfected with point-mutated CCR2. Membranes of transfected cells were incubated with 0.13 nM ^{125}I-MCP-1 in the presence of up to 10 μM antagonist and the pK_i was determined. pK_i values are expressed as ± standard error of mean (SEM) from at least three independent transfections (except where indicated: * represents $n = 2$). ia = inactive (no significant displacement of MCP-1 radioligand observed). NT = not tested. [b] Residues are identified according to the numbering scheme of Ballesteros and Weinstein.[29] The first number (1−7) represents the TM helix in which the residue is situated. The second number is the position of the residue in that helix, relative to the most highly conserved residue of the rhodopsin family, which is numbered 50. These are the asparagine of TM1, the arginine of TM3, and the proline of TM7.

Table 4. Profile of Antagonists across Double Mutant CCR2 Receptors[a]

	pK_i				
receptor variant	**1** (SB-282241)	**2** (RS-504393)	**3** (TAK-779 base)	**4** (TAK-779)	**5** (Teijin)
WT	7.00 ± 0.09	6.66 ± 0.016	7.16 ± 0.10	8.16 ± 0.12	6.47 ± 0.04
Y120A-T292A	5.61 ± 0.05	ia	ia	5.87 ± 0.14	ia
H121A/T292A	5.68 ± 0.63	ia	5.32 ± 0.08	6.74 ± 0.10	ia

[a] HEK 293 cells were transiently transfected with point−mutated CCR2. Membranes of transfected cells were incubated with 0.13 nM ^{125}I-MCP-1 in the presence of up to 10 μM antagonist and the pK_i was determined. pK_i values are expressed as ± standard error of mean (SEM) from at least three independent transfections. ia = inactive (no significant displacement of MCP-1 radioligand observed).

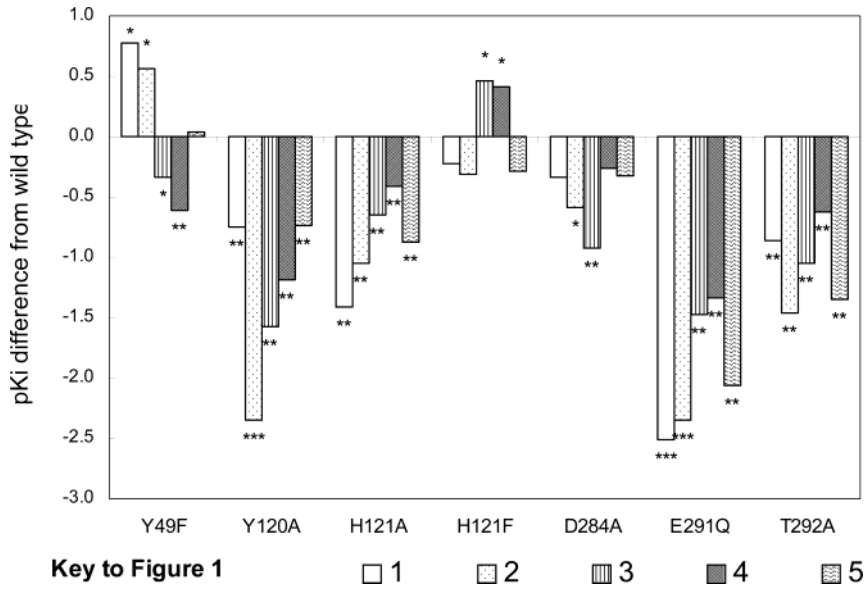

Figure 1. Summary of pK_i differences for compounds **1**−**5** on mutant CCR2 receptors compared to wild type CCR2[a].

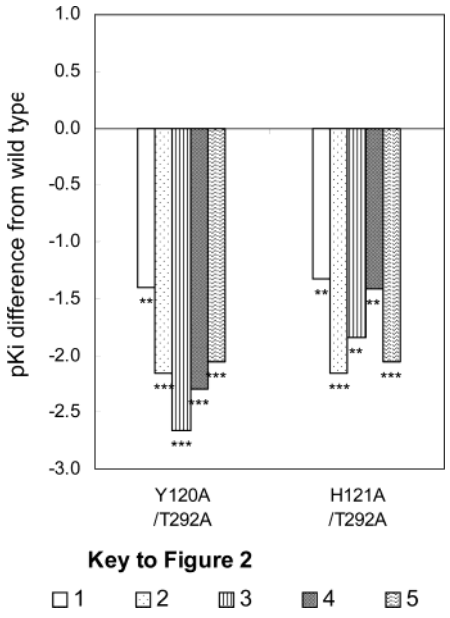

Figure 2. Summary of pK_i differences for compounds **1**−**5** on double mutant CCR2 receptors compared to wild type CCR2[a].

finities at H121F. Conversely, binding of compounds **3** and **4** are only affected to a minor extent at the H121A receptor mutant, but they intriguingly show a significant, albeit small, increase in affinity at H121F. This implies that the Takeda analogues **3** and **4** have a different mode of interaction with His 121 compared to the other compounds being studied. Finally, the effects of the CCR2 antagonists at the Y49F mutant receptor also show a pattern consistent with different binding modes for the different chemical classes. Thus, both **1** and **2** possess enhanced affinity at this Y49F mutant receptor, while **3** and **4** show slightly reduced affinity, and **5** displays no change in affinity. Similar effects were observed with a Y49L mutant receptor (data not shown).

Since major changes in affinities were observed with the Y120A, H121A, and T292 mutations, it was of interest to see if any of these effects were additive by looking at double mutations (see Table 4 and Figure 2).

In Figure 2 it can be seen that additive effects on lowering affinity of the antagonists are observed at all the double mutant receptors Y120A−T292A and H121A−T292A, with the exception of compound **1** at the H121A−T292A variant. This provides further evidence that amino acid residues in positions 120, 121, and 292 are closely involved with the binding of antagonists **1**−**5** to the CCR2 receptor.

Discussion

Initial Pharmacophore Generation and Ligand Docking. One of the goals of this work was to define a pharmacophore for small molecule ligands of the CCR2 receptor that could be used in the search of our "in-house" databases for novel lead series. Despite the structural diversity of the ligands studied here, it was recognized that they do have several common features. In addition to the basic center, all molecules contain at least two hydrophobic/aromatic sites. They all also contain an amide type carbonyl that could act as a hydrogen-bond acceptor. Given that only five compounds

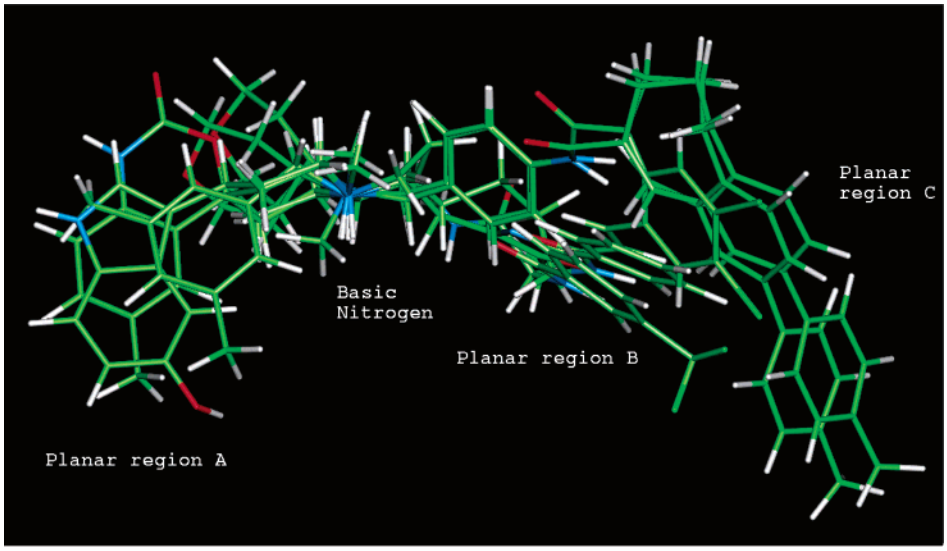

(a)

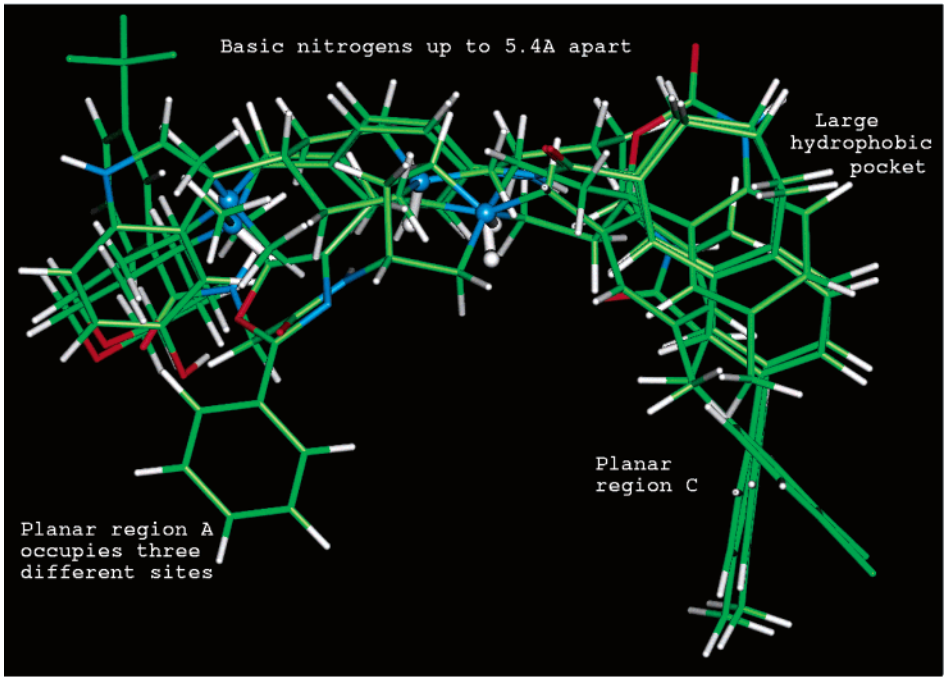

(b)

Figure 3. (a) Pharmacophore model based on rms fit of key presumed binding features. (b) Revised pharmacophore model based on overlap of the docked structures in the homology receptor model.

were being studied, a manual rms fit was made of these features. Overlap of the basic nitrogens and two aromatic centers was readily identified for the compounds, but it was impossible to find a fit for the carbonyl oxygens (see Figure 3a). The lack of overlap of the amido carbonyls could suggest that they played a structural rather than hydrogen-bonding role in the receptor, or simply that they bind to different H-bond donors. The best hypothesis obtained with the pharmacophore searching program Catalyst[24] showed an overlap of the aromatic rings of compounds **1**, **2**, **4**, and **5** and predicted two hydrogen-bond acceptors. Unfortunately, it took no account of the essential basic nitrogens. Search of our databases with these pharmacophores failed to produce any useful hits other than compounds closely related to the four series used in their generation (results not shown). We therefore decided to study their binding in more detail by docking them into the first CCR2 receptor model described in the Experimental Section. The intention was to confirm the binding hypotheses for these ligands with SDM experiments.

Ligand docking into receptor or enzyme structures has been a major topic of research for many years. Due to its importance in the drug design field, many programs have been developed for the automated docking of ligands into these structures. Such programs have the advantage of being much faster than manual docking. Because of their speed, however, they often suffer from the problem of assuming a fixed protein structure, without allowing for the influence of ligand-induced fit. A few programs do allow some flexibility of side chains, but none allow any major movement of the backbone, which is frequently observed from crystal structures. They also use some simplified scoring func-

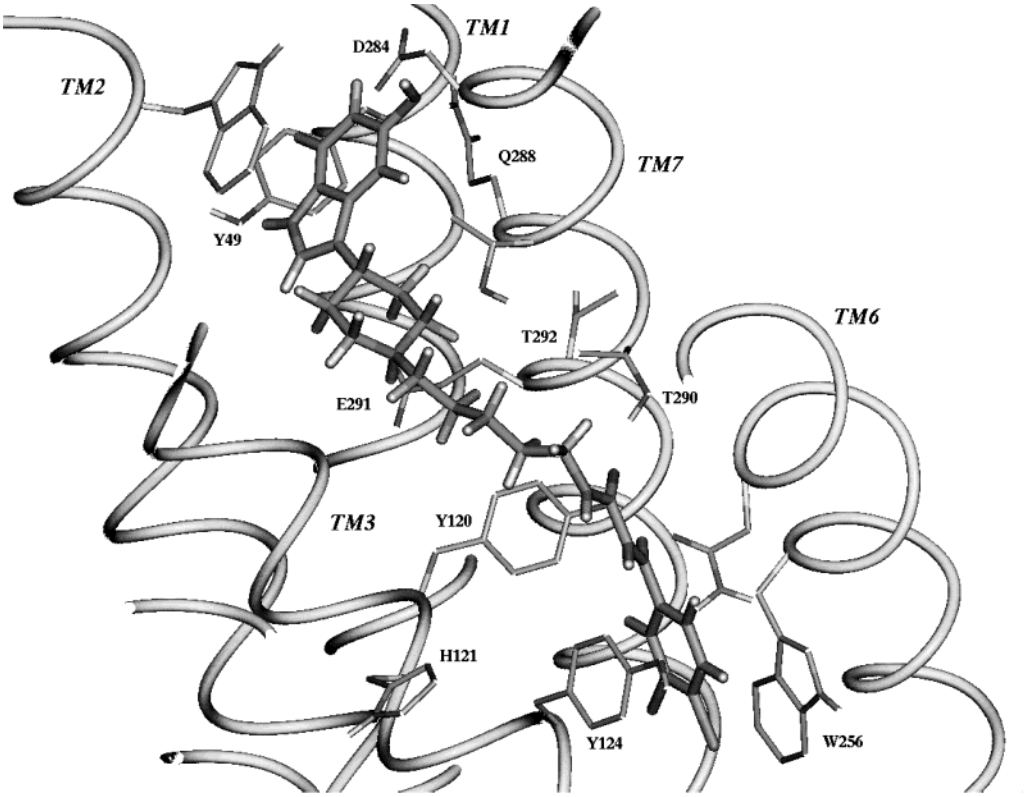

Figure 4. Initial docking of SB-282241 into the theoretical model of CCR2. This shows the binding pocket and the various residues chosen for the mutation studies.

tion to rank dockings rather than a computationally more expensive full energy minimization with potential inclusion of entropy terms. Their great advantage is that they are fast and can therefore handle hundreds or even thousands of compounds in a reasonable time. In our laboratories, we have studied the use of FlexX,[30] DOCK,[31] GOLD,[32] DockIt,[33] ICM-Dock,[34] and FLO[35] with varying degrees of success. The latter in particular allows some degree of side chain flexibility in the protein. They usually work best for systems with large accessible binding sites, a situation that is not commonly found in 7TM receptor models. Given the fact that only five ligands were being studied here and that the intention was to design suitable SDM experiments and use the results to "fine-tune" the dockings, it was felt that manual docking experiments were preferable in this case. These allowed complete freedom of placement of each ligand in the light of knowledge from the experimental results as well as the use of optimized ligand geometries, proper ab initio electrostatic descriptors, and full controlled flexibility of both the ligand and the protein.

Early Docking Models and the Design of Mutants. At the outset of this study, little evidence was available to confirm that the various ligands were bound in the TM domain. However, there is a wealth of SDM data from other GPCR proteins that supports the binding of small molecule (ant)agonists within the helix bundle.[36] This, together with the general lipophilic nature of the compounds, led us to construct early binding models, where the ligands were placed in the extracellular part of the TM bundle. As all the compounds studied contain a positively charged basic center, an acidic residue was sought as the primary binding site for these. CCR2 has a glutamate at the top of TM2 close to the first extracellular loop, and an aspartate and glutamate on the extracellular side of TM7. Initial extensive docking studies with SB-282241 and RS-504393 suggested that of these three residues, only the TM7 glutamate could form salt bridge complexes, where the remaining part of the ligands formed favorable interactions with the TM bundle (see Figure 4). Both compounds showed hydrogen-bonding interactions with polar residues in TM7 such as aspartate D284, glutamine Q288, and threonine T290. T290, for example, was predicted to hydrogen bond to the essential amide carbonyl of SB-282241. Another interesting observation with SB-282241 was that the indole NH of SB-282241 formed a hydrogen bond with the hydroxyl of tyrosine Y49 on TM1. The first round of mutation studies carried out was based on these two docking models. The mutants that were constructed were E291Q, D284A, Q288A, T290A and Y49F. Both compounds showed a reduction in binding of over 100-fold with the E291Q mutant, confirming that this is indeed the primary binding site of these compounds. On the other hand, with the exception of a small decrease in affinity with the D284A mutant, no significant effect on binding was seen with the other TM7 mutants (Q288A and T290A). These results with the glutamine and aspartate, which are one and two helical turns, respectively, above the key glutamate, would suggest that the ligands are buried more deeply in the receptor pocket than the models predicted. The lack of effect on binding with the mutant T290A on any of the ligands suggested that either the amide was playing a structural role in maintaining some geometrical requirement for fit or

possibly that another residue was responsible for hydrogen bonding to the carbonyl.

The flexible nature of the alkyl linking chain in SB-282241 allowed it to adopt a second conformation where it could hydrogen bond to histidine H121 on TM3. The initial dockings of RS-504393 and TAK-779, however, suggested that these ligands were not hydrogen bonding to the histidine but rather formed aromatic−aromatic π interactions with these ligands. Interestingly, the Teijin analogue **5** was not predicted to interact with this histidine. Mutation of the histidine (H121A) did indeed result in a reduction in binding of all five compounds. To further test the feasibility of all the ligands forming aromatic π interactions with H121, the mutation H121F was carried out. The effect on binding with this mutant was much less than H121A in the case of compounds **1**, **2**, and **5**. On the other hand, the H121F mutation resulted in a significant increase of about 0.5 pK_i log units for the Takeda compounds **3** and **4**, suggesting that an important increase in the aromatic π interaction was occurring in this region. Of particular interest is the fact that the corresponding residue in the CCR5 receptor is phenylalanine. This is one of the few differences between CCR2 and CCR5 in the TM domain, and these compounds are both more potent at CCR5.

The initial dockings of the Takeda and Teijin compounds postulated a hydrogen-bonding role for threonine T292 to the tetrahydropyran oxygen in **3** and **4** and to one of the peptide backbone carbonyls of **5**. No role for this residue was predicted, however, for compounds **1** and **2**. The mutation T292A resulted in a significant reduction in binding for all five compounds as can be seen in Figure 1. The dockings also showed that a large face to face aromatic interaction was predicted for compounds **3** and **4** with tyrosine Y120 in TM3. This was weaker in compounds **1** and **2** and was predicted not to have an effect with the Teijin compound **5**. This was the last of the mutations to be carried out in the work described here. As with the T292A mutation, the change of Y120A resulted in a large decrease in affinity for all five compounds.

Perhaps the most suprising result in this series of mutations was that of the TM1 tyrosine Y49F. The tyrosine hydroxyl was predicted to bind to the indole NH; hence, mutation to a phenylalanine should result in a reduction in observed binding. Instead, a significant increase was observed with both compounds. Indeed, with other analogues of SB-282241, this increase was found to be greater than 100-fold.[37] As this effect is evidently not due to a hydrogen bond between the receptor and the ligand, it must be the result of a broken hydrogen bond in the receptor itself. This could result in either the release of an adjacent side chain that is involved in a H-bond with the tyrosine or in the release of the aromatic ring itself, to form an interaction with the ligand. Alternatively, it could be speculated that the release of the tyrosine results in the rearrangement of several residues that then form a new binding pocket for the ligands. In the model, tyrosine Y49 does form a hydrogen bond with the TM7 glutamine Q288, but movement of residues upon mutation did not suggest any explanation for the observed increase in binding.

From these results, we had to conclude that while some aspects of the binding could be explained for each compound studied, no binding mode was in complete agreement with all the mutation data. Further refinements in the model were therefore necessary.

Refinement of the Receptor Ligand Binding Models. As mentioned previously, it was at this time that the first crystal structure of a Family A GPCR, viz. bovine rhodopsin, was published.[26] An homology model of the CCR2 receptor, based on this structure, was therefore used in an attempt to refine the binding modes of the five ligands, in a manner that would explain the observed SDM data. While the theoretically derived model and the crystal structure based homology model were quite close in many regions, some notable differences could be observed.

One such region of difference was the environment around the histidine H121. The altered orientation of TM5 in the homology model now meant that this histidine was involved in a strong hydrogen-bond interaction with the arginine R206 (R5:42) in TM5. Indeed, this arginine also formed an additional hydrogen bond with a second histidine, H202 (H5:38), one turn above it in TM5 (Figure 5a). Thus, mutation of H121 to either alanine or phenylalanine would not only alter potential interactions with the side chain itself, but might also have an indirect effect by releasing the arginine to form alternative interactions with ligands in its own right.

Another crucial difference between the homology model and its earlier theoretical counterpart was observed in the vicinity of tyrosine Y49. As with most amino acids, the tyrosine side chain prefers to lie in one of three rotameric states around the Cα−Cβ bond. In the homology model, the tyrosine sits in the most preferred state and in doing so the hydroxyl forms a strong hydrogen bond with glutamate E291, thus locking it in this rotameric form (Figure 5b). The mutation Y49F removes this hydrogen bond and allows the side chain to adopt one of the other two rotameric states if necessary. As will be seen shortly, this fact allowed us to develop a rationale for the observed increase in binding of the SB and Roche compounds, **1** and **2**. Also in the homology model the TM7 aspartate D284 forms a salt bridge with lysine K38 (K1:28) (see Figure 5a). Mutation of this aspartate as in D284A would increase the positive charge in that local region and thus decrease the strength of the salt bridge between the ligands and glutamate E291, thus explaining the observed slight decrease in affinity. The effect would be expected to be least in the quaternary center of TAK-779, where the electropositive charge is distributed over the molecule. Ab initio electrostatic potential calculations show that the positive charge on the quaternary center is, not suprisingly, centered mainly on those hydrogens β to the nitrogen (see Figure 6)

As with the earlier docking experiments, multiple initial orientations were considered in the starting conformations. The "best" orientations were chosen, however, not only on the basis of calculated interaction energy but also on the observed interactions with those residues that had been shown to be important from the SDM studies.

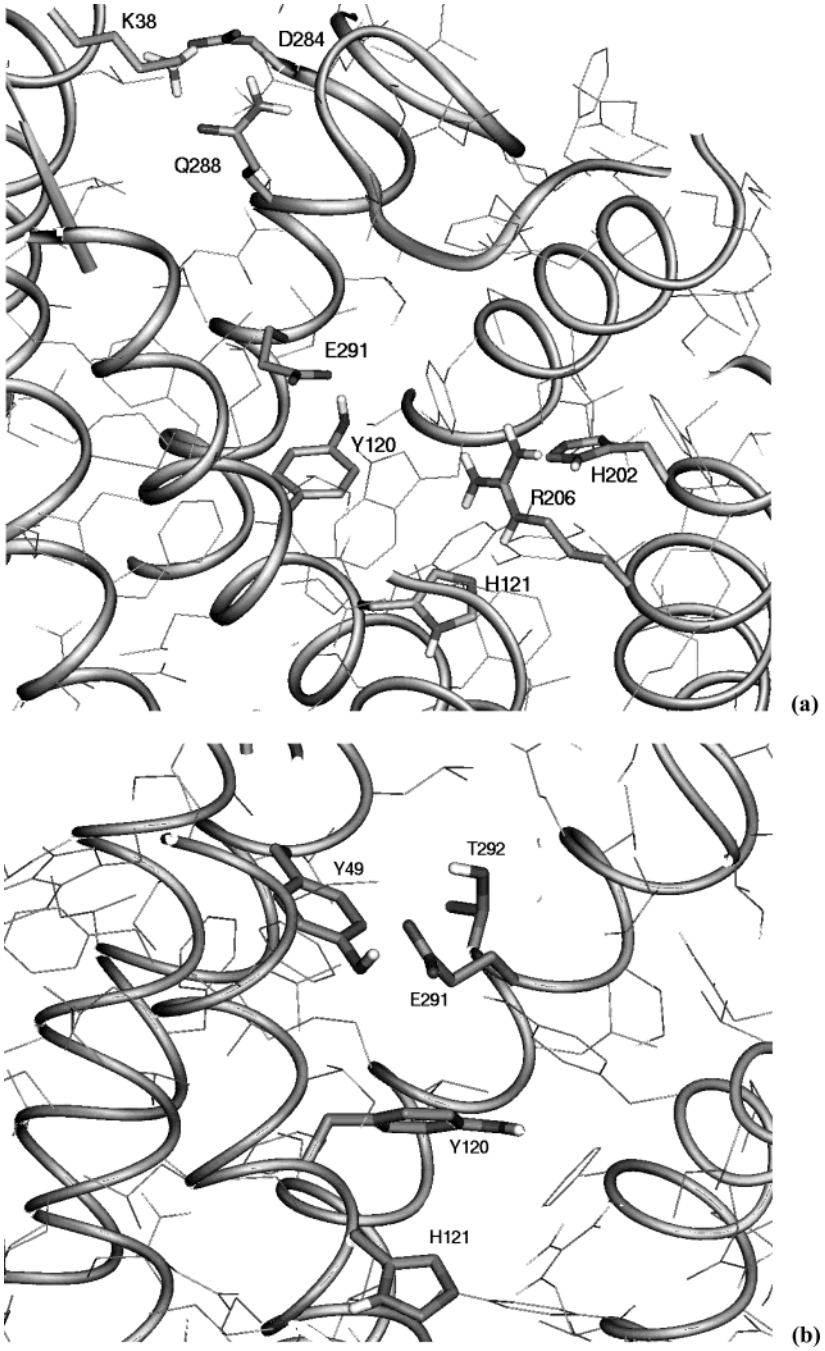

Figure 5. (a) CCR2 homology model showing the hydrogen-bonding network between histidines H121 and H202 and arginine R206. At the top the salt bridge between aspartate D284 and lysine K38 can be seen. (b) Binding pocket residues in the CCR2 homology model. Tyrosine Y49 can be seen in its preferred rotameric state, hydrogen bonded to glutamate E291.

Revised Docking of RS-504393. As before and with all compounds, the primary interaction was between the charged amino group and the carboxyl of glutamate E291. The bicyclic dihydrobenzoxazinone ring is sandwiched between the two aromatic residues on TM3, forming a coplanar π-stacked interaction with tyrosine Y120 and an orthogonal aromatic−aromatic interaction with histidine H121 (Figure 7). Mutation of both these residues to alanine would be expected to significantly decrease the binding, and this is indeed observed. The small loss of binding seen with the H121F mutation might seem suprising at first, but as previously noted, the histidine is rigidly held in a hydrogen bond with arginine R206 (R5:42). Replacement of the histidine by a phenylalanine causes a small steric clash with this arginine, which results in the phenylalanine moving away from an ideal interaction with the ligand. As can be seen from Figure 7, the oxazole ring forms a hydrogen bond with threonine T292, and again this is supported by the decrease in binding observed with the T292A mutant. The other main observation is that the 2-phenyl substituent on the oxazole is locked into the pocket normally occupied by the tyrosine Y49. It is necessary for this side chain to adopt the gauche + rotameric state. This is also seen with SB-282241 (see below) and is supported by the observed increase in binding of these two compounds with the Y49F mutant.

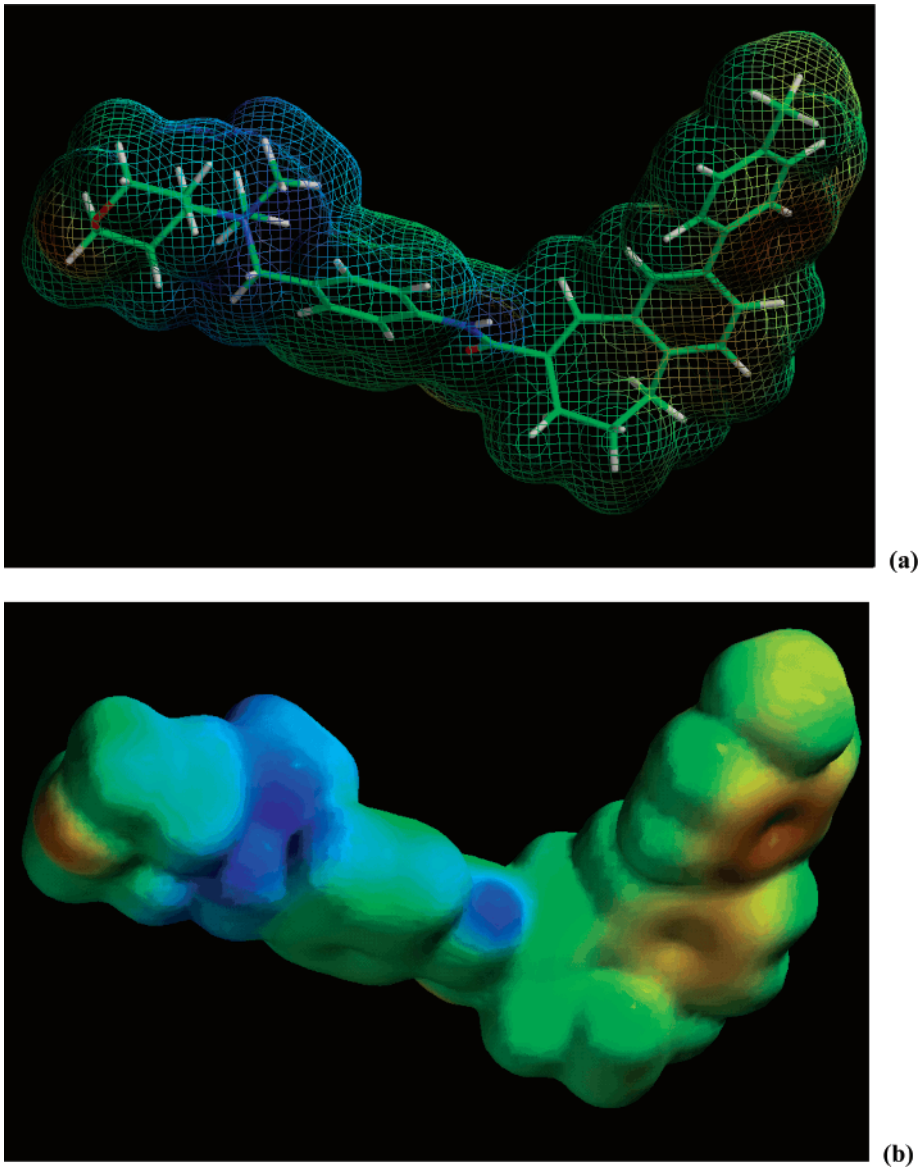

Figure 6. Electrostatic potential of TAK-779 calculated on the electron density surface and displayed in both (a) transparent and (b) opaque forms. In panel b in particular, the blue electropositive region of the quaternary center can be seen widely diffused over the surface.

Revised Binding of SB-282241. As with the Roche compound, it was found that tyrosine Y49 had to reorient to accommodate the indole ring of SB-282241. By binding in this pocket it was found that the 5-hydroxyl group formed a hydrogen bond with threonine T292. The protonated nitrogen of the piperidine forms a particularly strong interaction with glutamate E291, as evidenced also by the large decrease on binding with the E291Q mutant. This orientation of the indole piperidine allows the alkyl chain to adopt a low-energy conformation that places the dichlorocinnamide group in the aromatic pocket of TM3 (Figure 8). The tyrosine ring of Y120 does not form an aromatic−aromatic interaction with the dichlorophenyl group. Instead, it forms a hydrophobic interaction with the olefinic bond of the cinnamide. Thus, the effect of the Y120A mutation is smaller than is observed with the Roche or Takeda compounds. The main interaction in this pocket is an orthogonal π-aromatic binding with histidine H121. This is evidenced by the loss of binding with H121A and the much smaller change with the H121F mutants.

Binding of the Takeda Compound TAK-779 and Its Tertiary Amino Analogue. Compared to the dockings based on the earlier theoretical model of CCR2, both the Takeda free base (**3**) and quaternary TAK-779 (**4**) interacted with glutamate E291 on TM7 (the earlier model had suggested that E291 bound preferentially to the amide NH in the quaternary analogue). The tetrahydropyran ring of both compounds forms a favorable hydrophobic interaction with tyrosine Y49 in TM1. This is further enhanced in the quaternary compound **4**, because the increased positive charge of the hydrogens, β to the nitrogen, interacts favorably with the oxygen of the tyrosine hydroxyl (Figure 9). Thus the greater potency of the quaternary compound is readily explained. Mutation of this tyrosine to phenylalanine results in a loss of both effects, which is reflected in the lowering of observed binding, with the greater loss, as expected, in the quaternary analogue. Both Takeda compounds have the tetrahydropyran oxygen hydrogen-bonded to the TM7 threonine T292. In the tertiary analogue, the closer proximity of the nitrogen to

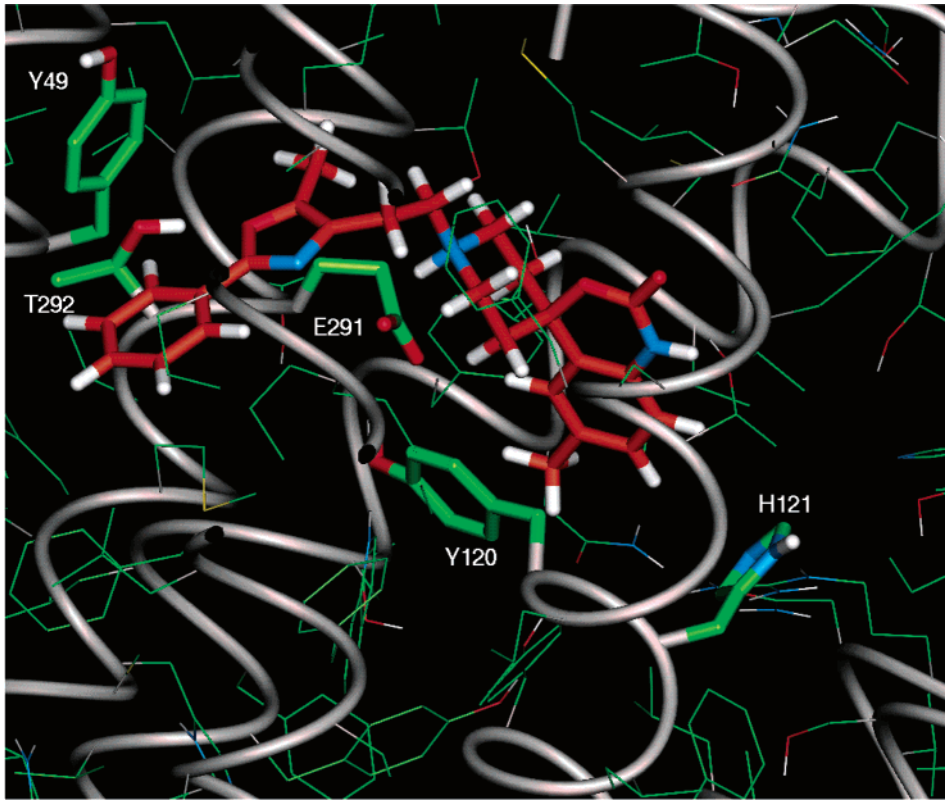

Figure 7. Docking of RS-504393 into the CCR2 homology model. Note in particular the less favored rotameric state of tyrosine Y49 necesssary to accommodate the phenyloxazole moiety in its pocket.

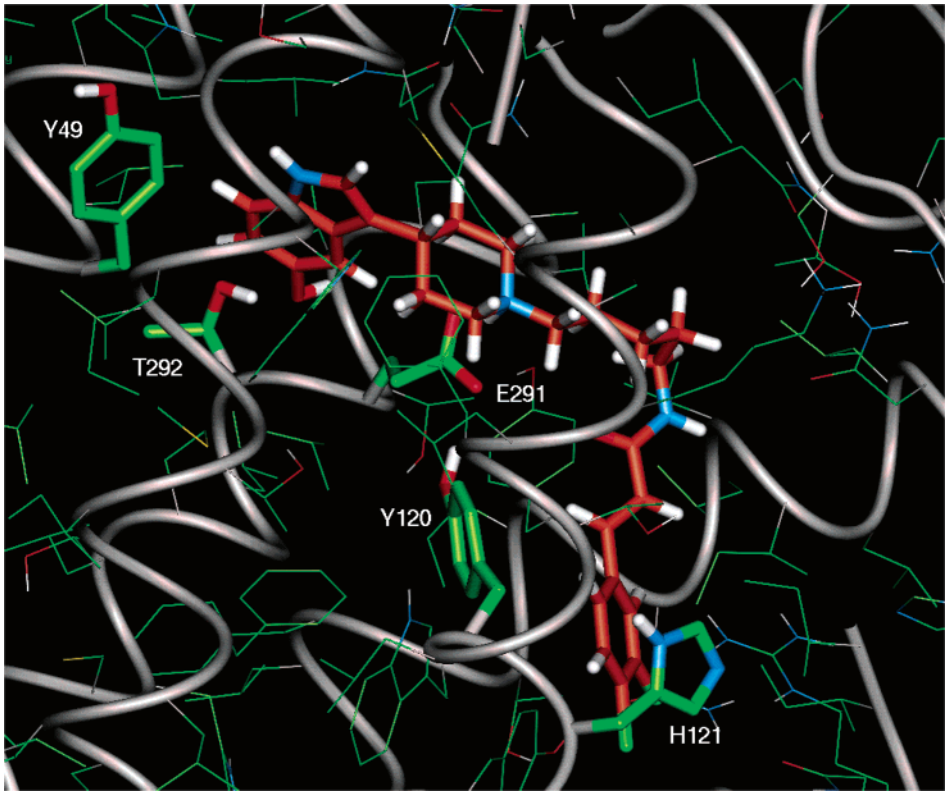

Figure 8. Revised docking of SB-282241 into CCR2. Once again, tyrosine Y49 must adopt the less favored gauche+ rotameric form to accommodate the indole. The 5-hydroxy group forms a hydrogen bond with threonine T292.

glutamate E291 means that the ring oxygen is also closer to threonine T292 than in the quaternary salt. This is reflected in the observed smaller loss of binding of TAK-779 with the T292A mutation. The biaryl rings are sandwiched between the tyrosines Y120 and Y259 (Y6:51) (on TM6) and to a lesser extent histidine H121. The interaction of this histidine with the TM5 arginine R206 means that there is only a weak aromatic–aromatic binding between the ligands and the histidine. Mutation of this residue to alanine would leave a cavity,

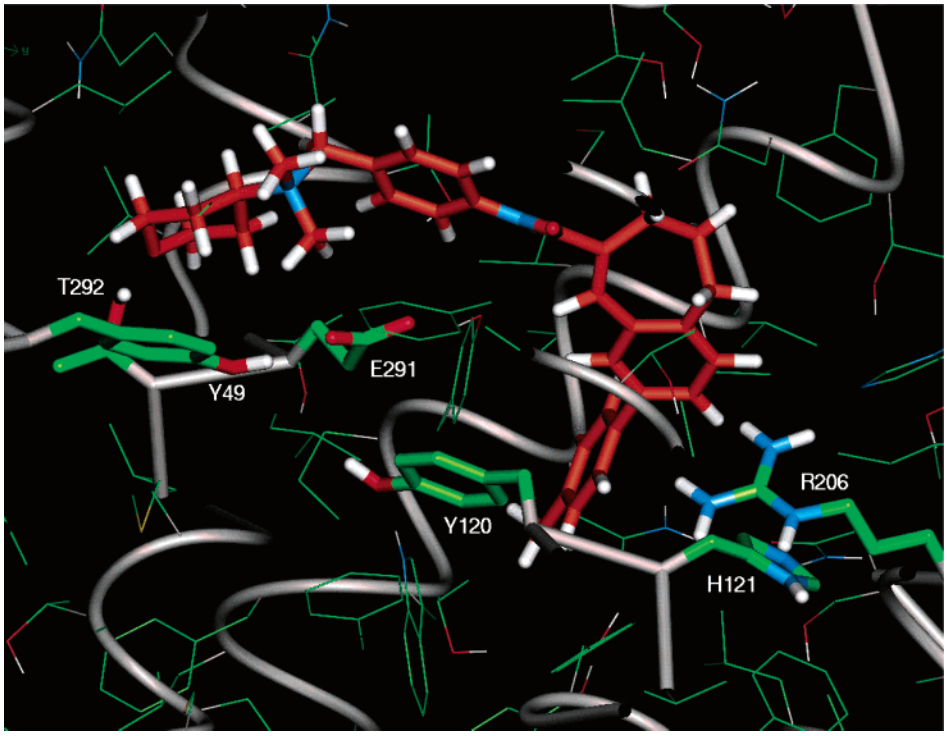

Figure 9. Binding of TAK-779 to CCR2. The $\pi\angle\pi$ aromatic interaction of the ligand with histidine H121 is weakened by the latter's H-bond to arginine R206. The corresponding phenylalanine in CCR5 does not have this interaction and can therefore adopt the alternative rotameric conformation and increase the $\pi-\pi$ interaction.

which would result in a lowering of binding, although as observed, this effect is less than with the other compounds that have a stronger direct binding to H121. On the other hand, the mutation H121F would allow the phenylalanine to stack with the biaryl rings, increasing the binding. This is reflected in the small but significant increase observed on binding the Takeda compounds. In the CCR5 receptor histidine H121 is a phenylalanine. The H121F switch is one of the main differences between the CCR2 and CCR5 receptors in the transmembrane domain, and is reflected in the increased potency of the Takeda compounds at the latter target, for which they were originally synthesized.

Revised Binding of the Teijin Compound 5. The Teijin lead compound was found to form a series of hydrogen-bonding interactions along its peptide backbone. Thus, in addition to the salt bridge with the pyrrolidine nitrogen, glutamate E291 also formed an interaction with the amide NH attached to the ring. The carbonyl of this amide also formed a hydrogen bond with the hydroxyl of tyrosine Y49, but this was at the expense of breaking the interaction between Y49 and E291, with no net gain in free energy. Thus, this is in keeping with the observed lack of effect with the Y49F mutation. The electronegative trifluoromethyl group has a favorable electrostatic interaction with lysine K38 (K1:28), which itself forms the salt bridge to aspartate D284. Threonine T292 also formed a strong hydrogen bond with the second amide carbonyl (Figure 10). The 2,4-dimethylphenyl ring does not extend fully into the TM3 aromatic pocket, and the main interactions are more hydrophobic in nature, between one of the methyl groups and the rings of tyrosine Y120 and histidine H121. This is reflected in the smaller drop in binding observed between this compound and the Y120A and H121A mutants, compared to the other compounds studied.

It can be concluded from the above results that the revised docking hypotheses for the five compounds studied are in good agreement with all the SDM experimental data. In particular, the binding modes for SB-282241 and RS-504393 explain the unusual increase with the Y49F mutant. The decrease in binding of the Takeda compounds with this mutant and the slight but significant increase with H121F can also clearly be explained. The binding pocket available for ligands in the CCR2 is quite extensive, and while all the compounds studied share common features, such as interactions with glutamate E291 and threonine T292, they differ in the way they interact with the aromatic pocket around TM3 and with the region at the top of TM1. The clear definition of this pocket with the combination of docking and SDM experiments has enabled us to develop a reliable model of the CCR2 receptor. In particular, it has allowed us to refine the original pharmacophore model used in the database searches. Thus, by extracting the five structures as they are docked into the receptor, the new overlay (Figure 3b) shows significant differences from that produced previously (Figure 3a). In particular, the nitrogen atoms in the five ligands are not superimposed but can be as much as 5.4 Å apart. Although they all bind to the same glutamate, this is not suprising in retrospect, because the glutamate is seen to adopt two low-energy rotameric states depending on the ligands bound. The models and revised pharmacophore are being used currently in the design of novel antagonist ligands for this important pharmaceutical target.

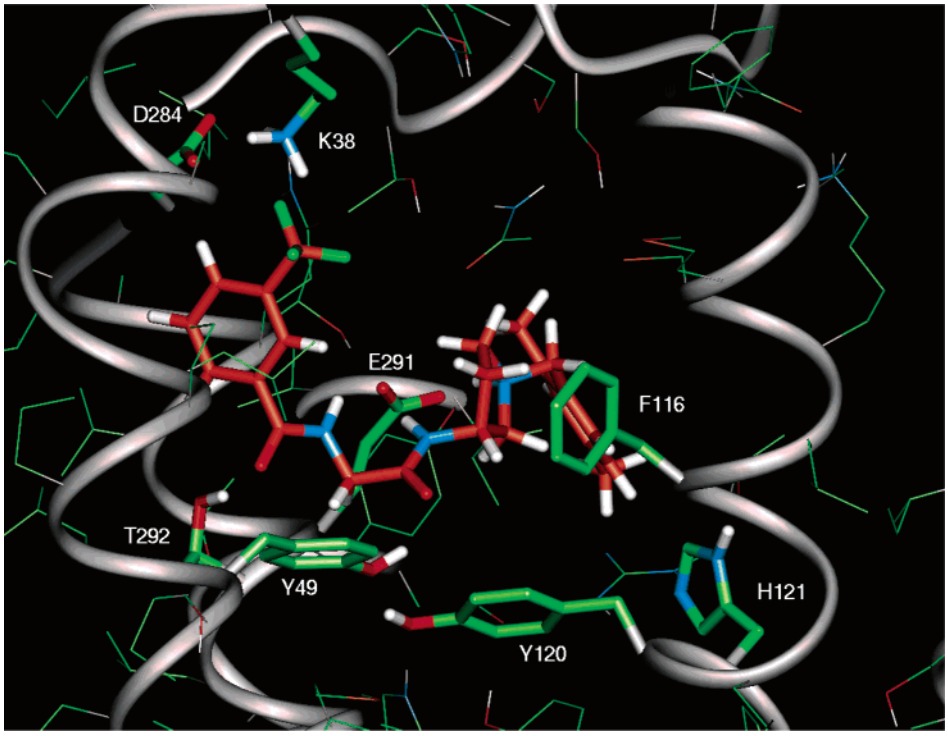

Figure 10. Docking of compound 5 (Teijin) in the CCR2 homology model. Note the hydrogen bonds from threonine T292 and tyrosine Y49 to the ligand backbone carbonyls. There is also a favorable electrostatic interaction between the trifluoromethyl group and lysine K38.

Summary and Conclusions

Using a theoretically derived model of the CCR2 receptor, the binding of the various key antagonist series described to date was studied, and plausible binding modes were defined for each. These were used as the basis for the design of a number of SDM experiments, which would verify (or not) the proposed hypotheses. The results of the SDM showed that while various aspects of the ligand interactions could be rationalized, the binding modes overall were clearly not in agreement with the experimental data and further refinements in the model would be necessary. The publication of a crystal structure of the related G-protein-coupled receptor bovine rhodopsin allowed us to construct a new model of CCR2. While the two models were close in many aspects, some key differences were apparent and these were shown to have important influences on the binding modes. The various ligands were reevaluated in the light of this model and the experimental SDM results. In this way plausible binding modes were developed for all compounds, which were in complete agreement with the SDM data. The new models highlight a potential problem in the design of pharmacophores in that the latter often overemphasize the importance of direct overlap of key binding features such as basic centers, because they assume a common binding mode with no major motions of the protein molecule. Currently these models are being used in the design of further novel antagonists. This work and the effects of these compounds on the various mutant receptors will be described in a future paper in this series.

Experimental Section

Chemistry. NMR spectra were determined with Bruker AC-200, AC-250, or AM-400 spectrometers using tetramethylsilane as internal standard. Electron impact mass spectra were determined using a Fisons VG 302 single quadrupole mass spectrometer. Elemental analysis were within 0.4% of the theoretical values. Tetrahydrofuran (THF) and *N*,*N*-dimethylformamide (DMF) were purchased from Aldrich as anhydrous solvents. Other solvents and reagents were of standard commercial grade and used without purification. Organic extracts were dried over anhydrous sodium sulfate before evaporation at reduced pressure. Chromatography was performed using commercially available Biotage silica cartridges or using Merck Art. 7734 silica gel.

(*E*)-*N*-(5-Bromopentyl)-3-(3,4-dichlorophenyl)acrylamide (7). A solution of 5-aminopentanol (42.3 g, 0.41 mol), *N*,*N*-diisopropylethylamine (72 mL), and dichloromethane (750 mL) was cooled (ice bath) and treated with 3,4-dichlorophenylacrylolyl chloride (47.7 g, 0.37 mol) in dichloromethane (150 mL) over 10 min and then the solution was stirred for a further 20 min. The solvent volume was reduced to (ca. 300 mL), water (1 L) was added, and the solid was collected (99.65 g). A sample of this solid (15.1 g, 0.05 mol) was suspended in dichloromethane (250 mL) containing carbon tetrabromide (18.3 g, 0.055 mol). Triphenylphosphine (14.1 g, 0.055 mol) was added in portions over 1 h, then the solution was stirred for 3 h. The solution was poured onto a flash silica column that was eluted with dichloromethane to give the title as a white solid that crystallized from hexane (15.96 g): ^{1}H NMR ($CDCl_3$) δ 1.6 (4H, m), 1.9 (2H, m), 3.4 (4H, m), 5.82 (1H, br t), 6.36 (1H, d, J = 17 Hz), 7.31 (1H, m), 7.46 (1H, d, J = 17 Hz), 7.56 (2H, m); MS *m*/*e* 364, 366 (MH^+).

(*E*)-3-(3,4-Dichlorophenyl)-*N*-{5-[4-(5-methoxy-1*H*-indol-3-yl)-piperidin-1-yl]pentyl}acrylamide (8). A stirred mixture of 4-(5-methoxyindol-3-yl)piperidine (1.15 g, 5.0 mmol), bromide **7** (2.0 g, 5.5 mmol and sodium hydrogen carbonate (1.0 g) in dimethylformamide (30 mL) was heated at 80 °C for 7 h. The reaction mixture was allowed to cool, poured onto brine, and extracted twice with ethyl acetate. The combined organic layers were washed with brine, dried, and evaporated to afford the crude product. Chromatography on a Biotage cartridge eluting with 3−6% methanol in dichloromethane containing 0.5% aqueous ammonia afforded **2** (2.3 g, 89%) as an off-white solid: ^{1}H NMR ($CDCl_3$) δ 1.39−1.55 (2H, m),

1.55−1.70 (4H, m), 1.81−2.3 (6H, m), 2.4−2.51 (2H, m), 2.75−2.91 (1H, m), 3.12 (2H, d, J = 12 Hz), 3.42 (2H, q, J = 7 Hz), 3.88 (3H, s), 5.89 (1H, b s), 6.39 (1H, d, J = 15 Hz), 6.86 (1H, dd, J = 9 and 2 Hz), 6.96 (1H, d, J = 2 Hz), 7.08 (1H, d, J = 2 Hz), 7.2−7.33 (2H, m), 7.40 (1H, d, J = 8 Hz), 7.51 (1H, d, J = 15 Hz), 7.57 (1H, m), 7.89 (1H, b s); MS *m/e* 514, 516 (MH^+).

(*E*)-3-(3,4-Dichlorophenyl)-*N*-{5-[4-(5-hydroxy-1*H*-indol-3-yl)-piperidin-1-yl]pentyl}acrylamide (1). A stirred mixture of **2** (1.0 g, 1.9 mmol) and pyridine hydrochloride (3.0 g) was heated in a sealed tube to 130 °C for 48 h. The reaction mixture was digested in methanol/chloroform, washed with aqueous ammonia and brine, dried, and evaporated to afford the crude product. Chromatography on a Biotage cartridge eluting with 6% methanol in dichloromethane containing 0.5% aqueous ammonia afforded **2** (375 mg, 40%) as an off-white solid: ^{1}H NMR (DMSO) δ 1.2−1.8 (7H, m), 1.8−2.1 (4H, m), 2.2 (2H, m), 2.6−2.7 (1H, m), 2.97 (2H, d, J = 10 Hz), 3.1−3.2 (3H, m), 6.58 (1H, dd,, J = 9 and 2 Hz), 6.71 (1H, d, J = 15 Hz), 6.83 (1H, d, J = 2 Hz), 6.95 (1H, d, J = 2 Hz), 7.10 (1H, d, J = 10 Hz), 7.40 (1H, d, J = 15 Hz), 7.58 (1H, dd, J = 9 and 2 Hz), 7.69 (1H, d, J = 10 Hz), 7.85 (1H, d, J = 2 Hz), 8.10 (1H, t, J = 7 Hz), 8.50 (1H, s), 10.41 (1H, s); MS *m/e* 500, 502 (MH^+). Anal. ($C_{27}H_{31}N_3O_2Cl_2$) C, H, N.

1′-[Spiro{4*H*-3,1−6-methylbenzoxazine-4,4′-piperidine}-2(1*H*)-one]carbamic Acid *tert*-Butyl Ester (10). A solution of *N*-BOC-2-bromo-4-methylaniline (2.86 g, 10 mmol) in dry tetrahydrofuran was cooled to 0 °C under argon. 1.5 M Methyllithium in tetrahydrofuran (8 mL, 12 mmol) was added dropwise over 5 min, and the mixture stirred for 30 min. After cooling the solution to −78 °C, 1.7 M *tert*-butyllithium (13 mL, 20 mmol) was added dropwise, and stirring continued for 1 h. A solution of *N*-BOC-4-piperidone (1.99 g, 10 mL) in tetrahydrofuran (5 mL) was added, and the solution was then allowed to warm to room temperature. Potassium *tert*-butoxide (50 mg) was added, and the mixture stirred for 17 h at room temperature. The reaction mixture was poured onto brine and extracted twice with ethyl acetate. The combined organic extracts were washed with brine, dried and evaporated to afford the crude product. Chromatography on silica using 30−60% ethyl acetate in hexane afforded **10** (1.7 g, 52%) as an off-white solid: ^{1}H NMR ($CDCl_3$) δ 1.49 (9H, s), 1.8−2.1 (4H, m), 2.31 (3H, s), 3.33 (2H, m), 4.14 (2H, m), 6.72 (1H, d, J = 9 Hz), 6.91 (1H, s), 7.05 (1H, m), 8.06 (1H, b s); MS *m/e* 331 ($M-H^+$).

6-Methylspiro{4*H*-3,1-benzoxazine-4,4′-piperidin}-2(1*H*)-one Hydrochloride (11). The *N*-BOC intermediate **10** (1.7 g, 5.1 mmol) was dissolved in ethanol saturated with hydrogen chloride. After stirring for 1 h, the solution was evaporated to dryness to afford **11** (1.3 g, 95%) as a light brown foam: ^{1}H NMR (DMSO) δ 2.1−2.4 (4H, m), 2.27 (3H, s), 3.0−3.2 (2H, m), 3.25−3.4 (2H, m), 8.30 (1H, d, J = 8 Hz), 6.98 (1H, s), 7.12 (1H, m), 9.0 (2H, b s), 10.25 (1H, b s); MS *m/e* 233 (MH^+).

1′-[2-(5-Methyl-2-phenyloxazol-4-yl)ethyl]-6-methylspiro{4*H*-3,1-benzoxazine-4,4′-piperidin}-2(1*H*)-one (2). The amine **11** (1.0 g, 3.7 mmol) was dissolved in dimethylformamide (20 mL) containing 4-bromoethyl-5-methyl-2-phenyl-1,3-oxazole (1.0 g, 3.7 mmol) and sodium hydrogen carbonate (1.0 g). The reaction mixture was heated to 60 °C for 4 h, allowed to cool, poured onto brine, and extracted twice with ethyl acetate. The combined organic layers were washed with brine, dried, and evaporated to afford the crude product. Chromatography on a Biotage cartridge eluting with 5% methanol in dichloromethane containing 0.5% aqueous ammonia afforded **2** (1.2 g, 78%) as an off-white solid: ^{1}H NMR ($CDCl_3$) δ 2.1−2.2 (4H, m), 2.30 (3H, s), 2.35 (3H, s), 2.6−3.95 (8H, m), 7.15 (1H, d, J = 8 Hz), 6.9−7.05 (2H, m), 7.4−7.44 (3H, m), 7.98−8.0 (2H, m), 8.29 (1H, b s); MS *m/e* 418 (MH^+). Anal. ($C_{25}H_{27}N_3O_3$) C, H, N.

[(*R*)-1-(2,4-Dimethylbenzyl)pyrrolidin-3-yl]carbamic Acid *tert*-Butyl Ester (14). A solution of 2,4-dimethylbenzaldehyde (1.5 g, 11 mmol), *R*-3-*tert*-butyloxycarbonylaminopyrrolidine (2.0 g, 10.7 mmol) in dichloroethane (40 mL) was treated with sodium triacetoxyborohydride (4.5 g). The mixture was stirred for 3 h and then poured onto aqueous sodium carbonate solution. Extraction with dichloromethane and washing the organic extracts with water followed by evaporation afforded the crude product. Purification was effected by chromatography on a Biotage cartridge eluting with 5% methanol in dichloromethane containing 0.5% aqueous ammonia afforded **14** (2.9 g, 89%): ^{1}H NMR ($CDCl_3$) δ 1.43 (9H, s), 1.56−1.58 (1H, m), 2.1−2.3 (2H, m), 2.33 (3H, s), 2.31 (3H, s), 2.51−2.58 (2H, m), 2.76 (1H, m), 3.53 (2H, s), 4.14 3.53 (2H, s), 4.14 (1H, b s), 4.84 (1H, b s), 6.9−7.03 (2H, m), 7.23 (1H, d, J = 8 Hz); MS *m/e* 304 (MH^+).

{[(*R*)-1-(2,4-Dimethylbenzyl)pyrrolidin-3-ylcarbamoyl]-methyl}carbamic Acid *tert*-Butyl Ester (15). The *N*-BOC compound **14** (2.9 g, 9.5 mmol) was dissolved in ethanol saturated with hydrogen chloride. After stirring for 1 h, the solution was evaporated to dryness to afford the corresponding amine dihydrochloride (2.5 g, ∼100%) as a light brown foam. This material was dissolved in dimethylformamide (30 mL) and added to a solution of diisopropylethylamine (2.6 mL), *N*-BOC-glycine (1.84 g, 10.5 mmol), *N*-hydroxybenzotriazole (1.6 g, 10.5 mmol), and diisopropylcarbodiimide (1.3 g, 10.5 mmol) in dimethylformamide (20 mL). The solution was stirred for 18 h and then poured onto brine. The mixture was extracted with ethyl acetate, and the combined organic layers were washed with sodium carbonate solution and brine, dried, and evaporated to afford the crude product. Purification was effected by chromatography on a Biotage cartridge eluting with 2−5% methanol in dichloromethane containing 0.5% aqueous ammonia to afford **15** (1.9 g, 56%) as an off-white foam: ^{1}H NMR ($CDCl_3$) δ 1.44 (9H, s), 1.6−1.63 (1H, m), 2.2−2.26 (2H, m), 2.29 (3H, s), 2.32 (3H, s), 2.5−2.54 (2H, m), 2.81−2.87 (1H, m), 3.54 (2H, s), 3.72 (2H, d, J = 6 Hz), 4.44 (1H, m), 5.04 (1H, m), 6.30 (1H, m), 6.92−6.97 (2H, m), 7.10 (1H, d, J = 8 Hz); MS *m/e* 362 (MH^+).

2-Amino-*N*-[(*R*)-1-(2,4-dimethylbenzyl)pyrrolidin-3-yl]-acetamide Dihydrochloride (16). The *N*-BOC compound **15** (1.9 g, 5.26 mmol) was dissolved in ethanol (40 mL) saturated with hydrogen chloride. After stirring for 2 h, the solution was evaporated to dryness to afford the corresponding amine dihydrochloride **16** (1.8 g, ∼100%) as a light brown foam: MS *m/e* 262 (MH^+); This material was used directly in the next step.

***N*-{[(*R*)-1-(2,4-Dimethylbenzyl)pyrrolidin-3-ylcarbamoyl]methyl}-3-methylbenzamide (5).** A solution of the amine **16** (334 mg, 1.0 mmol) in dimethylformamide (3 mL) was added to a solution of diisopropylethylamine (0.6 mL), 3-trifluoromethylbenzoic acid (210 mg, 1.1 mmol), *N*-hydroxybenzotriazole (170 mg, 1.1 mmol), and diisopropylcarbodiimide (140 mg, 1.1 mmol) in dimethylformamide (5 mL). The solution was stirred for 18 h and then poured onto brine. The mixture was extracted with ethyl acetate, and the combined organic layers were washed with sodium carbonate solution and brine, dried, and evaporated to afford the crude product. Purification was effected by chromatography on a Biotage cartridge eluting with 2−5% methanol in dichloromethane containing 0.5% aqueous ammonia to afford **5** (230 mg, 53%) as an off-white foam: ^{1}H NMR ($CDCl_3$) δ 2.2−2.4 (3H, m), 2.29 (3H, s), 3.30 (3H, s), 2.5−2.62 (2H, m), 2.85−2.91 (1H, m), 3.55 (2H, q, J = 13 Hz), 4.08 (2H, d, J = 8 Hz), 4.79 (1H, m), 6.45 (1H, d, J = 13 Hz), 6.9−7.15 (4H, m), 7.54 (1H, dd, J = 12 Hz), 7.75 (1H, d J = 12 Hz), 7.98 (1H, d, J = 12 Hz), 8.09 (1H, s); MS *m/e* 434 (MH^+). Anal. ($C_{23}H_{26}N_3O_2F_3$) C, H, N.

Site-Directed Mutagenesis. All oligonucleotides were synthesized by Sigma-Genosys Ltd (Pampisford, U.K.). Full-length cloning of the wild-type MCP-1/CCR2 gene has been published.[3] Mutants Y49F, Y120A, H121A, H121F, D284A, Q288A, E291Q, T292A, Y120A/T292A, and H121A/T292A were introduced using the QuickChange PCR-based mutagenesis kit (Stratagene) according to the manufacturer's protocol, using the wild-type expression vector, pCDNA3.1-MCP1, as the template for mutagenesis. The accuracy of all PCR-derived sequences was confirmed by dideoxy sequencing of the mutant plasmids.

Primer sequences (base changes introducing the mutations are italic):

Y49FFOR	CTCCTGCCTCCGCTC*TTC*TCGCTGGTGTTCATC
Y49FREV	GATGAACACCAGCGA*GAA*GAGCGGAGGCAGGAG
Y120AFOR	TTATTCACAGGGCTG*GCT*CACATCGGTTATTTTGG
Y120AREV	CCAAAATAACCGATGTG*AGC*CAGCCCTGTGAATAA
H121AFOR	TTCACAGGGCTGTAT*GCC*ATCGGTTATTTTGGC
H121AREV	GCCAAAATAACCGAT*GGC*ATACAGCCCTGTGAA
H121FFOR	TTCACAGGGCTGTAT*TTC*ATCGGTTATTTTGGC
H121FREV	GCCAAAATAACCGAT*GAA*ATACAGCCCTGTGAA
D284AFOR	CCAGTCAACTG*GCC*CAAGCCACGCAGG
D284AREV	CCTGCGTGGCTTG*GGC*CAGTTGACTGG
Q288AFOR	GACCAAGCCACG*GCG*GTGACAGAGACTC
Q288AREV	GAGTCTCTGTCAC*CGC*CGTGGCTTGGTC
E291QFOR	GCCACGCAGGTGACA*CAG*ACTCTTGGGATGACT
E291QREV	AGTCATCCCAAGAGT*CTG*TGTCACCTGCGTGGC
T292AFOR	CACGCAGGTGACAGAG*GCT*CTTGGGATGACTCAC
T292AREV	GTGAGTCATCCCAAG*AGC*CTCTGTCACCTGCGTG
H121A/Y120AFOR	CAAATTATTCACAGGGCTGGCCGCCATCGGTTATTTTGGCGG
H121A/Y120AREV	CCGCCAAAATAACCGATGGCGGCCAGCCCTGTGAATAATTTG

Transfection and Membrane Preparation. Mutant and wild type CCR2 receptor cDNA, subcloned into the mammalian expression vector pcNA3.1, were transiently transfected into 50−80% confluent HEK-293T cells using lipofectAMINE Plus (Life Technologies, Inc.) together with a cocktail of plasmids expressing human G-proteins (Gqi5, Gqo5, Gγs5, Gα15, and Gα16 all in pCDN expression vector) according to the manufacturer's protocol. Forty-eight hours posttransfection, cells were harvested and suspended into 10 mM HEPES pH 7 with 0.25 M sucrose, 1 mM EDTA, and 1 μg/mL each of pepstatin, antipain, aprotonin, and leupeptide. Cells were disrupted by sonication (Soniprep 150, GallenKamp) and cell debris was removed by low-speed centrifugation, 500*g* for 15 min, 4 °C (Beckman GS-6R centrifuge). The resulting supernatant was spun at 105 000*g* for 22 min, 4 °C (Beckman L8-70M Ultra centrifuge), the pellet resuspended in the same buffer, and the centrifugation was repeated. The final membrane was resuspended in assay buffer (50 mM Hepes pH 7.4, 1 mM $CaCl_2$, 5 mM $MgCl_2$) and stored at −80 °C.

Radioligand Binding Assay. Saturation binding studies were performed with increasing concentrations of ^{125}I-MCP-1 (0.02−2 nM, Bolton and Hunter labeled, Amersham, specific activity = 2000 Ci/mmol) to membrane protein, (cell equivalent of 200 000 cells/well) in binding buffer with 0.5% albumin fraction V (fatty acid free) and incubated for 2 h at room temperature. Membranes were harvested as described.[10] The K_d and B_{max} were determined by single site saturation curve fitting using GraFit 4 (Erithacus Software Ltd.). Nonspecific binding was determined by measuring binding of ^{125}I-MCP-1 to untransfected HEK 293 cell membranes or by incubation in the presence of 300 nM MCP-1. The binding displacement assay was performed as described previously.[10]

Chemotaxis Assay. The chemotaxis assay was essentially carried out as previously described.[3] Vehicle or compound were added/diluted from a 10 mM stock solution in DMSO, giving final concentrations in the range 10 nM to 10 μM, and 1 nM MCP-1 was used as the agonist.

Statistical Analysis. Differences between data for mutant and WT receptors for individual compounds were calculated along with their statistical significance based on *t*-tests using estimates of the standard deviation of the pIC_{50}/pK_i calculated by pooling the within-compound variation across all compounds for a particular mutant.

Acknowledgment. We are grateful to Deirdre Hickey for helpful discussions and Lynne Roxbee-Cox for skilled technical assistance. Special thanks are also due to Ian Wall for his help with the Catalyst program.

References

(1) Saunders: J.; Tarby, C. M. *Drug Discovery Today* **1999**, *4*, 80−92.

(2) Murphy, P. M.; Baggiolini, M.; Charo, I. F.; Hebert, C. A.; Horuk, R.; Matsushima, K.; Miller, L. H.; Oppenheim, J. J.; Power, C. A. International Union of Pharmacology. XXII. Nomenclature for Chemokine Receptors. *Pharmacol. Rev.* **2000**, *52*, 145−176.

(3) Berkhout, T. A.; Sarau, H. M.; Moores, K.; White, J. R.; Elshourbagy, E.; Apelbaum, E.; Makwana, J.; Foley, J. J.; Schmidt, D. B.; Imburgia, C.; McNulty, D.; Mathews, J.; O'Donnell, K.; O'Shannessy, D.; Scott, M.; Groot, P. H. E.; Macphee, C. Cloning, in Vitro Expression, and Functional Characterisation of a Novel Human CC Chemokine of the Monocyte Chemotactic Protein (MCP) Family (MCP-4) that Binds and Signals through the CC Chemokine Receptor 2B. *J. Biol. Chem.* **1997**, *272*, 16404−16413.

(4) (a) Ross, R. Atherosclerosis- An Inflammatory Disease. *New England J Med.* **1999**, *340*, 115−126. (b) Reape, T. J.; Groot, P. H. E.; Chemokines and Atherosclerosis. *Atherosclerosis* **1999**, *147*, 213−215.

(5) (a) Yla-Herttuala, S.; Lipton, B. A.; Rosenfeld, M. E.; Sarkioja, T.; Yoshimura, T.; Leonard, E. J.; Witztum, J. L.; Steinberg, D. Expression of Monocyte Chemotactic Protein in Macrophage-rich Areas of Human and Rabbit Atherosclerotic Lesions. *Proc. Natl. Acad. Sci. U.S.A.* **1991**, *88*, 5252−5256. (b) Takeya, M.; Yoshimura, T.; Leonard, E. J.; Takahashi, K. Detection of Monocyte Chemoattractant protein-1 in Human Atherosclerotic Lesions by an Anti-monocyte Chemoattractant Protein-1 Monoclonal Antibody. *Hum. Pathol.* **1993**, *24*, 534−539. (c) Nelken, N. A.; Coughlin, S. R.; Gordon, D.; Wilcox, J. N. Monocyte Chemotactic Protein-1 in Human Atheromatous Plaques. *J. Clin. Invest.* **1991**, *88*, 1121−1127. (d) Rayner, K.; Van Eersel, S.; Groot, P. H. E.; Reape, T. J. Localisation of mRNA for JE/MCP-1 and its Receptor CCR2 in Atherosclerotic Lesions of the ApoE Knockout Mouse. *J. Vasc. Res.* **2000**, *37*, 93−102.

(6) (a) Gu, L.; Okada, Y.; Clinton, S. K.; Gerard, C.; Sukhova, G. K.; Libby, P.; Rollins, B. J. Absence of Monocyte Chemotactic Protein-1 Reduces Atherosclerosis in Low-Density Lipoprotein-deficient Mice. *Mol. Cell.* **1998**, *2*, 275−281. (b) Boring, L.; Gosling, J.; Cleary, M.; Charo, I. F. Decreased Lesion Formation in CCR2-/- Mice Reveals a Role for Chemokines in the Initiation of Atherosclerosis. *Nature* **1998**, *394*, 894−897.

(7) Aiello, R. J.; Bourassa, P.-A. K.; Lindsey, S.; Weng, W.; Natoli, E.; Rollins, B. J.; Milos, P. M. Monocyte Chemoattractant Protein-1 Accelerates Atherosclerosis in Apolipoprotein E-deficient Mice. *Arteriosclerosis* **1999**, *19*, 1518−1525.

(8) Gong, J.-H.; Ratkay, L. G.; Waterfield, J. D.; Clark-Lewis, I. An Antagonist of Monocyte Chemoattractant Protein-1 (MCP-1) Inhibits Arthritis in the MRL-lpr Mouse Model. *J. Exp. Med.* **1997**, *186*, 131−137.

(9) Trivedi, B. K.; Low, J. E.; Carson, K.; LaRosa, G. J. Chemokines: Targets for Novel Therapeutics. In *Annual Reports in Medicinal Chemistry* Doherty, A. M., Ed.; Academic Press: New York, 2000; Vol. 35, pp 191−200.

(10) Forbes, I. T.; Cooper, D. G.; Dodds, E. K.; Hickey, D. M. B.; Ife, R. J.; Meeson, M.; Berkhout, T.; Gohil, J.; Moores, K. CCR2B Receptor Antagonists: Conversion of a Weak HTS Hit to a Potent Lead Compound. *Bioorg. Med. Chem. Lett.* **2000**, *10*, 1803−1806.

(11) Mirzadegan, T.; Diehl, F.; Ebi, B.; Bhakta, S.; Polsky, I.; McCarley, D.; Mulkins, M.; Weatherhead, G. S.; Lapierre, J.-M.; Dankwardt, J.; Morgans, D.; Wilhelm, R.; Jarnagin, K. Identification of the Binding Site for a Novel Class of CCR2B Chemokine Receptor Antagonists. *J. Biol. Chem.* **2000**, *275*, 25562−25571.

(12) (a) Shiraishi, M.; Kitayoshi, T.; Aramaki, Y.; Honda, S. WO Patent 99/ 32468. (b) Baba, M.; Nishimura, O.; Kanzaki, N.; Okamoto, M.; Sawada, H.; Iizawa, Y.; Shiraishi, M.; Aramaki, Y.; Okonogi, K.; Ogawa, Y.; Meguro, K.; Fujino, M. A Small Molecule Non-peptide CCR5 Antagonist with Highly Potent and Selective Anti-HIV Activity. *Proc. Natl. Acad. Sci. U.S.A.* **1999**, *96*, 5698−5703. (c) Shiraishi, M.; Aramaki, Y.; Seto, M.; Imoto, H.; Nishikawa, Y.; Kanzaki, N.; Okamoto, M.; sawada, H.; Nishimura, O.; Baba, M.; Fujino, M. Discovery of Novel, Potent, and Selective Small-molecule CCR5 Antagonists as Anti-HIV Agents: Synthesis and Biological Evaluation of Anilide Derivatives with a Quaternary Ammonium Moiety. *J. Med. Chem.* **2000**, *43*, 2049−2063.

(13) (a) Shiota, T. WO Patent 99/25686. (b) Tarby, C. M.; Endo, N.; Moree, W.; Kataioka, K.; Ramirez-Weinhouse, M. M.; Imai, M.; Bradley, E.; Saunders, J.; Kato, Y.; Meyers, P. In 218th National ACS Meeting in New Orleans, 1999, Poster Abstract No. 82.

(14) Shigenaga, S.; Manabe, T.; Matsuda, H.; Fujii, T.; Hiroi, J. Synthesis and Pharmacological Properties of N-[4-[4-(1H-indol-3-yl)piperidinoalkyl]-2-thiazolyl]alkanesulfonamides as Novel Antiallergic Agents. *Chem. Pharm. Bull.* **1993**, *41*, 1589−1595.

(15) Studies on **1** (unpublished), **2** (Lapierre, J. M. 26th National Medicinal Chemistry Symposium, 14−16 June, 1998, Richmond, VA), and **4** (ref 12c) have indicated that these small molecule antagonists are competitive inhibitors of ^{125}I-MCP-1 binding, so the expression of results as pK_i's and pK_b's is valid

(16) (a) Unger, V. M.; Hargrave, P. A.; Baldwin, J. M.; Schertler, G. F. X. Arrangement of rhodopsin transmembrane α-helixes**.** *Nature (London)* **1997**, *389*, 203−206. (b) Baldwin, J. M.; Schertler, G. F. X.; Unger, V. M. An alpha-carbon template for the transmembrane helixes in the rhodopsin family of G-protein-coupled receptors. *J. Mol. Biol.* **1997**, *272*, 144−164.

(17) Blaney, F. E.; Raveglia, Luca, F.; Artico, M.; Cavagnera, S.; Dartois, C.; Farina, C.; Grugni, M.; Gagliardi, S.; Luttmann, M. A.; Martinelli, M.; Nadler, G. M. M. G.; Parini, C.; Petrillo, P.; Sarau, H. M.; Scheideler, M. A.; Hay, D. W. P.; Giardina, G. A. M. Stepwise Modulation of Neurokinin-3 and Neurokinin-2 Receptor Affinity and Selectivity in Quinoline Tachykinin Receptor Antagonists. *J. Med. Chem.* **2001**, *44*, 1675−1689.

(18) Blaney, F. E.; Tennant, M. Computational tools and results in the construction of G protein-coupled receptor models. In *Membrane Protein Models;* Findlay, J. B. C., Ed.; Oxford, Bios Scientific Publishers Ltd., 1996; pp 161−176.

(19) Blaney, J. M.; Crippen, G. M.; Dearing, A.; Dixon, J. S.; Spellmeyer, D. C. DGEOM95. Available from the Quantum Chemistry Program Exchange, Bloomington, IN, 1995.

(20) Brooks, B. R.; Bruccoleri, R. E.; Olafson, B. D.; States, D. J.; Swaminathan, S.; Karplus, M. CHARMM: A program for macromolecular energy, minimization, and dynamics calculations. *J. Comput. Chem.* **1983**, *4*, 187−217. *CHARMm*, Version 25.2, Revision 98.0731; Accelrys Inc.: San Diego, CA, 1999.

(21) (a) Elber, R.; Karplus, M. Enhanced sampling in molecular dynamics: Use of the time-dependent Hartree approximation for a simulation of carbon monoxide diffusion through myoglobin. *J. Am. Chem. Soc.* **1990**, *112*, 9161−75. (b) Roitberg, A.; Elber, R. Modeling side chains in peptides and proteins: Application of the locally enhanced sampling and the simulated annealing methods to find minimum energy conformations. *J. Chem. Phys.* **1991**, *95*, 9277−87.

(22) *SPARTAN SGI*, version 5.1.3; Wave function Inc., 18401 Von Karman, Suite 370, Irvine, CA 92612, 1999.

(23) Clark, T.; Alex, A.; Beck, B.; Chandrasekhar, J.; Gedeck, P.; Horn, A.; Hutter, M.; Rauhut, G.; Sauer, W.; Steinke, T. *Vamp 7.0*; Oxford Molecular Ltd., 1998.

(24) *Catalyst*, v4.7 (579); Accelrys Inc.: San Diego, CA, 2002.

(25) Dunbrack, R. L., Jr.; Karplus, M. Backbone-dependent rotamer library for proteins. Application to side-chain prediction. *J. Mol. Biol.* **1993**, *230*, 543−74.

(26) Polczewski, K.; Kumasaka, T.; Hori, T.; Behnke, C. A.; Motoshima, H.; Fox, B. A.; Le Trong, I.; Teller, D. C.; Okada, T.; Stenkamp, R. E.; Yamamoto, M.; Miyano, M. Crystal structure of rhodopsin: A G protein-coupled receptor. *Science (Washington, D. C.)* **2000**, *289*, 739−745.

(27) (a) Bromidge, S. M.; Dabbs, S.; Davies, D. T.; Davies, S.; Duckworth, D. M.; Forbes, I. T.; Gaster, L. M.; Ham, P.; Jones, G. E.; King, F. D.; Mulholland, K. R.; Saunders, D. V.; Wyman, P. A.; Blaney, F. E.; Clarke, S. E.; Blackburn, T. P.; Holland, V.; Kennett, G. A.; Lightowler, S.; Middlemiss, D. N.; Trail, B.; Riley, G. J.; Wood, M. D. Biarylcarbamoylindolines Are Novel and Selective 5-HT2C Receptor Inverse Agonists: Identification of 5-Methyl-1-[[2-[(2-methyl-3-pyridyl)oxy]-5-pyridyl]carbamoyl]-6-trifluoromethylindoline (SB-243213) as a Potential Antidepressant/Anxiolytic Agent. *J. Med. Chem.* **2000**, *43*, 1123−1134. (b) Gaster, L. M.; Blaney, F. E.; Duckworth, D. M.; Ham, P.; Jenkins, S.; Jennings, A. J.; Joiner, G. F.; King, F. D.; Mulholland, K. R.; Starr, S.; Wyman, P. A.; Hagan, J. J.; Hatcher, J.; Jones, B. J.; Middlemiss, D. N.; Price, G. W.; Riley, G.; Roberts, C.; Routledge, C.; Selkirk, J.; Slade, P. D. The Selective 5-HT1B Receptor Inverse Agonist 1′-Methyl-5-[[2′-methyl-4′-(5-methyl-1,2,4-oxadiazol-3-yl)biphenyl-4-yl]carbonyl]-2,3,6,7-tetrahydrospiro-[furo[2,3-f]indole-3,4′-piperidine] (SB-224289) Potently Blocks Terminal 5-HT Autoreceptor Function Both in Vitro and in Vivo. *J. Med. Chem.* **1998**, *41*, 1218−1235.

(28) *Quanta98*, version 98.1111; Accelrys Inc.: San Diego, CA, 1999.

(29) Ballesteros, J. A.; Weinstein, H. Integrated methods for the construction of three-dimensional models and computational probing of structure−function relations in G-protein coupled receptors. *Methods Neurosci.* **1994**, *25*, 366−428.

(30) *FlexX*; Tripos, Inc., 1699 South Hanley Rd., St. Louis, MO.

(31) Ewing, T. J. A.; Kuntz, I. D.. Critical evaluation of search algorithms for automated molecular docking and database screening. *J. Comput. Chem.* **1997**, *18*, 1175−1189.

(32) *GOLD*; Cambridge Crystallographic Data Centre, 12 Union Rd., Cambridge CB2 1EZ, UK.

(33) *DockIt*; Metaphorics, LLC., 27401 Los Altos #360, Mission Viejo, CA, 92691.

(34) *ICM*, v2.7; MolSoft, San Diego, CA, 1998.

(35) *FLO*; Thistlesoft Inc., Morris Township, NJ.

(36) Bikker, J. A.; Trumpp-Kallmeyer, S.; Humblet, C. G-Protein Coupled Receptors: Models, Mutagenesis, and Drug Design. *J. Med. Chem.* **1998**, *41*, 2911−2927.

(37) Blaney, F. E.; et al. Manuscript in preparation.

JM030862L